



Contents lists available at ScienceDirect

Arabian Journal of Chemistry

journal homepage: www.ksu.edu.sa

Original article

Extraction process optimization of *Ligusticum chuanxiong* hort. and its cardiomyocyte-protective effects via regulation of Dvl-1/Akt/GSK-3 β /Nrf2Ling-Yu Wang^{a,b}, Dan-Dan Tang^a, Ruo-Lan Li^a, Mei-Yan Li^a, Li-Sha He^{a,*}, Xu-Feng Pu^{a,*}, Shu-Ting Zhao^{a,*}^a State Key Laboratory of Southwestern Chinese Medicine Resources/School of Pharmacy, School of Basic Medicine/School of Intelligent Medicine, Chengdu University of Traditional Chinese Medicine, No.1166 Liutai Avenue, Chengdu 611137, PR China^b Medical education department, Zhongjiang County Traditional Chinese Medicine Hospital, No.818 North section of the First Ring Road, Zhongjiang County, Deyang 618100, PR China

ARTICLE INFO

Keywords:

Ligusticum chuanxiong Hort.
Myocardial ischemia
Extraction process optimization
Apoptosis
Oxidative stress

ABSTRACT

Background: The traditional Chinese medicine *Ligusticum chuanxiong* Hort. (CHX) has been used in the management of heart disease, particularly myocardial ischemia (MI), but its related active constituents and mechanisms remain to be further explored.

Methods: We analyzed the blood entry constituents of CHX by UPLC-Q-TOF-MS/MS. The protective effects of the constituents on cardiomyocytes were evaluated using isoproterenol (ISO)-treated H9c2 cells to screen for quality markers (Q-markers) of CHX. We used a single-factor and orthogonal experimental design to optimize the extraction process of CHX based on Q-markers. Then, ISO-treated rats were prepared for evaluation of the anti-MI effects of CHX extracts via echocardiography, electrocardiography (ECG), H&E staining, Masson staining, TUNEL staining, and transmission electron microscopy (TEM). Furthermore, the potential mechanisms of CHX in ISO-treated H9c2 cells were explored via western blot assays, flow cytometry analysis, and immunofluorescence assays.

Results: A total of 7 blood entry constituents of CHX were identified. All 7 components had protective effects on H9c2 cells and were considered to be Q-markers of CHX. The optimal extraction parameters for CHX were as follows: extraction time, 1.5 h; solid-liquid ratio, 1:20; ethyl alcohol (EtOH) concentration, 80 %; and 3 extraction times. The ECG results showed that CHX could reduce ISO-induced ST segment elevation. Echocardiography revealed that CHX improved heart function and increased fractional shortening (FS) and ejection fraction (EF) in ISO-treated rats. H&E, Masson and TUNEL staining showed that CHX reduced inflammatory infiltration and cell necrosis in heart tissue and reduced cardiac tissue fibrosis and apoptosis. TEM analysis revealed that CHX decreased cardiomyocyte mitochondrial swelling and lipid droplet formation. The in vitro results showed that CHX can prevent apoptosis, protect the mitochondrial membrane potential (MMOP) and reduce oxidative stress in ISO-treated H9c2 cells. Western blot and immunofluorescence results indicated that the mechanism of the anti-MI effect of CHX was related to the regulation of the Dvl-1/Akt/GSK-3 β /Nrf2 pathway. The cellular protective effect of CHX can be inhibited by Akt inhibitor MK-2206.

Conclusion: Collectively, we optimized the extraction process of CHX, and the optimized CHX showed significant anti-MI effects via regulation of the Dvl-1/Akt/GSK-3 β /Nrf2 signaling pathway.

Abbreviations: AHP, Analytic Hierarchy Process; Akt, protein kinase B; ARE, Antioxidant response elements; Bax, Bcl2-associated X protein; BCA, Bradford protein assay; Bcl-2, B-Cell Leukemia/Lymphoma 2 protein; CHX, *Ligusticum chuanxiong* Hort.; CK-MB, Creatine kinase-MB; cTnT, Cardiac troponin T; Dvl-1, Dsh Homolog 1; ECG, Electrocardiogram; ECL, Enhanced chemiluminescence luminescence; EtOH, Ethyl alcohol; FBS, Fetal bovine serum; GSK-3 β , Glycogen synthase kinase-3 beta; GSH-Px, Glutathione peroxidase; H&E, Hematoxylin & Eosin; ISO, Isoproterenol; LDH, Lactate dehydrogenase; MDA, Malondialdehyde; MI, Myocardial ischemia; MMOP, Mitochondrial membrane potential; Nrf2, Nuclear factor erythroid 2-related factor; PBS, Phosphate buffer saline; PI3K, Phosphoinositide 3-kinase; PVDF, Polyvinylidene fluoride; SOD, Superoxide dismutase; TEM, Transmission electron microscope; TCM, Traditional Chinese medicine; TMP, Tetramethylpyrazine.

* Corresponding authors at: State Key Laboratory of Southwestern Chinese Medicine Resources, School of Pharmacy, School of Intelligent Medicine, School of Basic Medicine, Chengdu University of Traditional Chinese Medicine, Chengdu 611137, PR China.

E-mail addresses: helisha@cdutcm.edu.cn (L.-S. He), pxf68@263.net (X.-F. Pu), zhaoshuting@cdutcm.edu.cn (S.-T. Zhao).

<https://doi.org/10.1016/j.arabjc.2024.105843>

Received 26 February 2024; Accepted 21 May 2024

Available online 23 May 2024

1878-5352/© 2024 The Author(s). Published by Elsevier B.V. on behalf of King Saud University. This is an open access article under the CC BY-NC-ND license (<http://creativecommons.org/licenses/by-nc-nd/4.0/>).

1. Introduction

The American Heart Association reports that ischemic heart disease is the dominant cause of loss of life in the United States (Tsao et al., 2023). The occurrence of myocardial ischemia (MI) is mainly caused by diseases of the coronary artery system, such as atherosclerosis (Shao et al., 2020), coronary artery spasm or coronary microvascular disease (Matta et al., 2020; Rahman et al., 2019). Therefore, the use of vasodilators to increase blood supply, the reduction of myocardial oxygen consumption to protect the myocardium and the use of antithrombotic agents to prevent intracoronary thrombosis or dissolve thrombosis are strategies for the treatment of MI. These methods are effective at relieving symptoms of MI, but they can also have serious side effects. For example, the vasodilator nitroglycerin can cause hypotension (Stemple et al., 2021). In addition, antithrombotic drugs can cause damage to the digestive tract and allergic reactions (Li et al., 2020). Therefore, more medicines that can effectively treat MI without causing toxic side effects are urgently needed.

The occurrence of MI is often associated with oxidative stress, autophagy, Ca⁺ ion stabilization, inflammation, and cardiomyocyte apoptosis (Han et al., 2022; Li et al., 2018; Zhang et al., 2019). The signaling pathways involved include nuclear factor E2-related factor 2 (Nrf2)/HO-1, phosphoinositide 3-kinase (PI3K)/Akt and Wnt/ β -catenin (Zhang et al., 2022). In the PI3K/Akt/Nrf2 pathway, Akt is phosphorylated by PDK1, PDK2 binds to Ser473 and Thr308 to phosphorylate (p)-Akt, and p-Akt regulates cardiac recovery after myocardial infarction through downstream signaling pathways (Liu et al., 2024; Qian et al., 2024; Sarbassov et al., 2005). Nrf2 is a key regulatory factor that maintains redox balance and is involved in the initiation of downstream antioxidant enzyme transcription (Shen et al., 2019). Keap1 anchors Nrf2 in the cytoplasm under normal circumstances (Li et al., 2021a). Under conditions of uncontrolled redox balance, antioxidant response element (ARE) sequences bind to Nrf2, which is translocated to the nucleus to improve the antioxidant capacity of cells (Liao et al., 2020). Glycogen synthase kinase-3 beta (GSK-3 β) is a bridge between the Nrf2 and Akt pathways. GSK-3 β phosphorylates Nrf2 by excluding Nrf2 transcription factors from the nucleus (Salazar et al., 2006). However, the S9 site of GSK-3 β can be phosphorylated by activated Akt, and the ability of GSK-3 β to phosphorylate Nrf2 is lost (Yu and Xiao, 2021). GSK-3 β also participates in the Wnt/ β -catenin pathway, which is involved in heart damage repair. The Wnt signaling pathway is activated during the healing process and improves cardiac remodeling after myocardial infarction (Meyer et al., 2022). In addition, activation of the Wnt signaling pathway also promotes angiogenesis after myocardial infarction (Wang et al., 2022).

The management of traditional Chinese medicines (TCMs) for various diseases has a 5000-year history in China. The use of TCM has attracted worldwide attention in recent years because of its multicomponent and multitarget features (She et al., 2023; Peng et al., 2024). In Chinese medicine, MI is also known as a “chest impediment” and can be caused by blood stasis, cold coagulation, heart pulse and other factors. The commonly used herbal medicines for treating MI in TCM include *Salvia miltiorrhiza* Bge, *Panax notoginseng* (Burk) F. H. Chen, *Angelica sinensis* (Oliv.) Diels and *Ligusticum chuanxiong* Hort. (CHX) (Bu et al., 2020). In previous studies, CHX and its active constituents have been shown to be useful for the management of coronary artery diseases, particularly MI. CHX can protect mitochondria, improve energy metabolism, scavenge oxygen free radicals and inhibit apoptosis (Qian et al., 2014; Yin et al., 2021; Zheng et al., 2018; Zhang et al., 2015). Nevertheless, the active constituents and mechanisms of CHX remain to be further explored. The goal of our study was to optimize the extraction process of CHX and explore the anti-MI effect of CHX and its related mechanisms, which would be beneficial for the development of this herbal medicine as a clinical drug for treating cardiovascular diseases.

2. Materials and methods

2.1. Reagents

The rhizome of *Ligusticum chuanxiong* Hort. CHX was obtained from Sichuan New Lotus Decoction Slice Co., Ltd. (Chengdu, China) and was obtained from Associate Professor Wei Peng. The standard reference materials of ferulic acid, N-butylideneephthalide, senkyunolide I, ligustilide, senkyunolide H, butylphthalide and senkyunolide A were obtained from Sichuan Weikeqi Biological Technology Co., Ltd. (Chengdu, China). Sodium pentobarbital was obtained from Beijing Chemical Reagent Company. (Beijing, China). H9c2 cells were obtained from Wuhan Pu-nuo-sai Life Technology Co., Ltd. (Wuhan, China). We purchased penicillin–streptomycin, DMEM and 0.25 % trypsin-EDTA (1 \times) from Gibco Co. (Grand Island, NY, United States). Phosphate-buffered saline (PBS), Masson's Tri-Color Dyeing Solution and a DAB (SA-HRP) TUNEL kit were purchased from Wuhan Servicebio Biotechnology Co., Ltd. (Wuhan, China). We obtained assay kits for superoxide dismutase (SOD), glutathione peroxidase (GSH-Px), and malondialdehyde (MDA) from Suzhou Michy Biomedical Technology Co., Ltd. (Suzhou, China). Hematoxylin and eosin (H&E) were obtained from Biosharp Life Sciences. (Hefei, China). The primary antibodies against B-cell leukemia/lymphoma 2 protein (Bcl-2), Bcl-2-associated X protein (Bax), Dsh homolog 1 (Dvl-1), protein kinase B (Akt), Lamin B1, phosphorylated (p)-Akt, GSK-3 β , p-GSK-3 β , Nrf2, cleaved (C)-caspase-3, caspase-3, β -catenin, Wnt-1, Wnt-3, GAPDH, HPR- and fluorescence-conjugated secondary antibodies were obtained from ABclonal Biotech. Co., Ltd. (Wuhan, China). CCK-8, RIPA lysis buffer, SDS–PAGE protein loading buffer, and BCA protein assay reagents were acquired from Boster Biol. Tech. (Wuhan, China). Rat cardiac troponin T (cTnT), creatine kinase-MB (CK-MB) and lactate dehydrogenase (LDH) ELISA kits were obtained from Shanghai Zhucai Biotechnology Co., Ltd. (Shanghai, China). We obtained TransSerum EQ fetal bovine serum (FBS) from HyClone (Logan, UT, USA). We purchased an Annexin V-FITC/PI assay kit and enhanced chemiluminescence (ECL) reagent from 4A Biotech (Beijing, China). We obtained assay kits for DCFH-DA and JC-1 from US Everbright, Inc. (Suzhou, China). ISO was obtained from Shanghai RHAWN Chemical Technology Co., Ltd. (Shanghai, China). We obtained bovine serum albumin (BSA) from Shanghai Scigrace Biotech. Co., Ltd. (Shanghai, China). Diltiazem (Dil) was obtained from Zhejiang Yatai Pharmaceutical Co., Ltd. (Shaoxing, China).

2.2. Animals

SPF Sprague–Dawley (SD) rats aged 10–11 weeks and weighing 200 g \pm 20 g were obtained from Sipeifu Biotechnology Co., Ltd. (Beijing, China) (SCXK (Jing) 2019–0010). The rats were kept under controlled conditions with a room humidity of 55 % \pm 10 %, a temperature of 20 $^{\circ}$ C \pm 2 $^{\circ}$ C, free access to water and food, and a 12 h light/dark cycle. All animal experimental procedures were approved by the Experimental Animal Ethics Committee of Chengdu University of Traditional Chinese Medicine (Approval No. 2022–27) and complied with the ARRIVE guidelines.

2.3. Analysis of blood entry constituents of CHX

2.3.1. Preparation of CHX extracts

The dried CHX was pulverized into a coarse powder capable of passing through a 24-mesh sieve. Subsequently, we used 10 volumes of 80 % ethanol to extract 60 g of CHX coarse powder 2 times by reflux, and each extraction lasted for 1.5 h. The extraction solution was combined twice and concentrated under vacuum conditions with a rotary evaporator. Finally, the concentrated extract was freeze-dried to obtain CHX freeze-dried powder.

2.3.2. Preparation of CHX-containing serum

Eight male SD rats were orally administered 1200 mg/kg CHX. After continuous administration for 7 d, the rats were fasted for 12 h. After the last gavage, the rats were anesthetized by intraperitoneal injection of 3 % pentobarbital sodium (30 mg/kg), and blood was collected from the abdominal aorta. The whole blood samples were placed at room temperature and centrifuged to obtain the serum from the upper fraction. Three times the amount of methanol was added to the serum, which was mixed for 3 min and then centrifuged to remove the precipitated substance. A nitrogen blowing instrument was used to blow dry the liquid solvent from the serum samples. Finally, the serum samples were redissolved in 100 μ L of methanol to obtain CHX-containing serum samples.

2.3.3. Identification of CHX extracts and blood entry constituents

CHX freeze-dried powder was diluted to 50 μ g/mL with methanol. A 0.22 μ m microporous membrane was used to filter the CHX sample. Next, 5 μ L aliquots of the CHX sample and CHX-containing serum were analyzed with a Waters ACQUITY UPLC BEH C_{18} column (1.7 μ m, 2.1 \times 50 mm) at 35 $^{\circ}$ C using an ACQUITY UPLC I-Class PLUS system (Waters Corporation, Massachusetts, USA). The mobile phase consisted of 0.1 % phosphate water (A) and acetonitrile (B). The gradient elution program was as follows: 0–5 min, 10 % B; 5–12 min, 10–15 % B; 12–17 min, 15–20 % B; 17–33 min, 20–40 % B; 33–48 min, 40–80 % B; 48–50 min, 80–10 % B; and 50–55 min, 10 % B. The flow rate was 0.3 mL/min.

Using a Waters SYNAPT XS Quadrupole-Time-of-Flight Mass Spectrometer equipped with an electrospray ionization source (Waters Corporation, Massachusetts, USA), we performed mass spectrometry on the CHX sample and CHX-containing serum. In the range of m/z 100–1000, mass spectrometry was performed under the following conditions: capillary voltage, 3.0 kV; sample cone voltage, 40 V; source temperature, 150 $^{\circ}$ C; desolvent gas temperature, 450 $^{\circ}$ C; desolvent gas flow rate, 800 L/h; molecular ion scanning collision energy, 6 V; and MS/MS collision energy, 2–4 V. The composition was analyzed by MassLynx V4.2 software.

2.4. Effects of blood entry constituents on ISO-induced H9c2 cells

2.4.1. Cell culture

DMEM containing 10 % FBS, 1 % penicillin and streptomycin was used to cultivate H9c2 cells. The environment consisted of humid air with 5 % CO_2 at 37 $^{\circ}$ C. The medium was changed every two days. Cells were passed when they reached the exponential growth stage.

2.4.2. Iso-induced H9c2 cells

We cultivated H9c2 cells in 96-well plates (1 \times 10⁴ cells/well). When the cell growth reached 70–80 %, different concentrations (20, 40, 60, 80, and 100 μ g/mL) of ISO were used to treat the cells for 24 h. The culture medium was discarded, and the cells were incubated with 100 μ L of CCK-8 buffer (10 μ L of CCK-8 concentrate + 90 μ L of media) in each well under dark conditions for 30 min. Finally, the absorbance at 450 nm was measured using a microplate reader to determine the half maximal inhibitory concentration (IC₅₀) of ISO (Zhu et al., 2022).

Cell viability (%) = (measured value – blank value)/(normal value – blank value) \times 100 %.

The measured value refers to the absorbance value of the treatment group. The blank value refers to the absorbance value of the CCK-8 blank solution without cells. The normal value refers to the absorbance value of the normal cell group.

2.4.3. The effect of blood entry constituents on H9c2 cells

In 96-well plates, the cells were treated with ferulic acid (4, 8, 16, 32, or 64 μ g/mL), senkyunolide I (5, 10, 20, 40, or 80 μ g/mL), senkyunolide H (2, 4, 8, 16, or 32 μ g/mL), senkyunolide A (0.625, 1.25, 2.5, 5, 10 μ g/mL), butylphthalide (5, 10, 20, 40, 80 μ g/mL), ligustilide (2.5, 5, 10, 20, 40 μ g/mL), or N-butylidenephthalide (5, 10, 20, 40, or 80 μ g/mL) for 12

h and then treated with the IC₅₀ concentration of ISO for 24 h. Finally, the cell viability was measured by CCK-8 assay on a microplate reader.

2.5. Optimization of the extraction process of CHX

2.5.1. Preparation of the CHX sample and mixed reference solution

CHX extracts were diluted to 40 mg/mL with methanol. The standard reference materials of ferulic acid, senkyunolide A, senkyunolide I, N-butylidenephthalide, butylphthalide, senkyunolide H, and ligustilide were weighed accurately and dissolved in a 10 mL volumetric flask with methanol. Then, CHX mixed reference solutions with concentrations of 0.122, 0.848, 0.120, 0.178, 0.190, 0.125, and 0.674 mg/mL were obtained.

2.5.2. Methodology validation

We used a Thermo UltiMate 300 system (Thermo Fisher Scientific Inc., Massachusetts, USA) to detect the contents of the Q-markers in the CHX extract. Then, 0.1 % phosphate water (A) and acetonitrile (B) were combined to form the mobile phase. The elution procedure was performed at a rate of 1 mL/min and a temperature of 35 $^{\circ}$ C. The optimized gradient elution program is shown in Table S1, Supporting Information. The high-performance liquid chromatography (HPLC) chromatograms of the CHX sample and mixed reference solution are shown in Fig. S1, Supporting Information.

We used a CHX sample solution to verify the precision of the instrument, the method's repeatability, and the sample's stability. We used different concentrations of mixed reference solution to investigate the linear relationship of the Q-markers. The CHX sample solution and the mixed reference solution were mixed 1:1 to investigate the recovery rate.

2.5.3. Analytical hierarchy process (AHP) calculation of component weights

The contents of multiple components in CHX were observed, so we used the overall score method to evaluate the extraction rate of CHX. Based on the contents of Q-markers in CHX and relevant literature reports, the weights of each component were determined by the AHP method (Table S2, Supporting Information shows the judgment matrix scoring table), and the overall score was calculated.

2.5.4. Orthogonal experiment

First, we used a single-factor method to detect the impact of extraction time (A), solid–liquid ratio (B), ethyl alcohol (EtOH) concentration (C) and extraction time (D) on the extraction rate of CHX. Fig. S2, Supporting Information shows the results of the single-factor experiment. When the extraction time was 2.5 h, the CHX extraction rate did not increase; however, the extraction rate decreased when the extraction time was 3 h; this may be because the volatile components contained in CHX were transformed into other substances or volatilized under prolonged heating. Therefore, 1.5, 2 and 2.5 h were selected as the three extraction times. When the solid–liquid ratio was 1:15, the CHX extraction rate reached its peak. Therefore, in the orthogonal experiment, 1:10, 1:15, and 1:20 were selected as the three solid–liquid ratios. When the EtOH concentration was 80 %, the extraction rate of CHX no longer increased. Therefore, in the orthogonal experiment, 40 %, 60 %, and 80 % EtOH were selected as the three EtOH concentrations. When the number of extractions was 3, the CHX extraction rate did not increase. Therefore, in the orthogonal experiment, 1, 2 and 3 times were selected as the extraction times.

Then, 9 aliquots of CHX coarse powder (20 g each) were weighed. CHX was extracted by heating reflux according to the L₉(3⁴) orthogonal experimental design table. The obtained CHX extract was diluted to 40 mg/mL, filtered through a 0.22 μ m filter membrane, and analyzed by HPLC. Finally, we carried out a range analysis to determine the best extraction process for CHX according to the orthogonal experimental design results. The optimized extraction process was used to extract

CHX, and subsequent experiments were carried out.

2.6. Animal experiments

2.6.1. Grouping, modeling, and administration of animals

We divided 42 male SD rats (200 g \pm 20 g) into 6 groups: the normal group, ISO model group, positive drug Dil group, low-dose CHX group (600 mg/kg) (Li et al., 2014), medium-dose CHX group (900 mg/kg), and high-dose CHX group (1200 mg/kg). The formulation of the tested dosage of CHX in this study was based on its standard clinical dosage (6–10 g crude herb) (Committee, 2020), which was converted into a rat dosage according to body surface area. The CHX groups were given CHX freeze-dried powder extracted by an optimized process. The rats in the CHX groups were given the drug for 14 d (Xiao et al., 2019). On Days 1–12 of the experiment, the rats in the CHX groups were orally administered CHX extract according to their weight, while those in the normal group, model group, and Dil group were orally administered distilled water. The clinical dose of Dil was 3.2 mg/kg, which was translated to 20 mg/kg for rats. On Days 13–14 of the experiment, CHX and Dil were administered to the rats according to their weights. The rats in the normal group and model group were orally administered distilled water. On Days 13–14 of the experiment, rats in the model group, CHX groups and Dil group were intraperitoneally injected with ISO (40 mg/kg) to establish the MI model after 1 h of intragastric administration. Rats in the normal group were injected with normal saline.

2.6.2. Electrocardiogram (ECG) and echocardiography detection

On the 14th day of the experiment, the rats were anesthetized with pentobarbital sodium after ISO injection for 1 h. The rats were fixed in a supine position on a plane, and hypodermic needle electrodes were connected to the rat limb lead position II (Wu et al., 2019). A BL-420 N Biological Signal Collection and Analysis System (Taimeng, Chengdu, China) was used to record ECGs under stable baseline conditions.

A VEVO 3100 system (Visual Sound Wave, Toronto, Canada) was used to perform echocardiography to assess left ventricular function. In brief, the rats were placed on a temperature-controlled operating table in the supine position to maintain a stable heart rate. After hair removal and application of an ultrasound gel to the chest area of the rats, left ventricular function on the parasternal long axis was assessed using M-mode imaging, and echocardiographic measurements were performed (Zhou et al., 2022).

2.6.3. Cardiac index determination

After the ECGs and echocardiograms of the rats were assessed, the weights of the rats were recorded. After blood was collected from the aorta of each rat, the rats were euthanized by cervical dislocation. Complete rat heart tissue was isolated and cleaned. The weight of the heart tissue was recorded, and the cardiac indices of the rats were calculated.

$$\text{Cardiac index} = \text{Heart weight (g)}/\text{Rat body weight (g)}.$$

2.6.4. Serum and myocardial tissue biochemical examinations

The whole blood sample was centrifuged, and the serum was extracted from the upper fraction. The LDH, CK-MB, cTnT, MDA, SOD and GSH-Px levels in the serum were detected according to the manufacturer's instructions.

The left ventricular tissues were removed from each group of rats and cut after weighing. After adding cooled PBS (tissue:PBS = 1:9) to the tissue, tissue homogenization was performed with an ice bath for 30 min. The homogenate was centrifuged, and the supernatant was collected. The levels of MDA, SOD and GSH-Px in cardiac tissue were detected according to the manufacturer's instructions.

2.6.5. Histopathological analysis of the left ventricle

We fixed heart tissue for 24 h with 4 % paraformaldehyde. Then, the heart tissue was dehydrated with gradient concentrations of alcohol

successively and dipped in wax. The wax-impregnated heart tissue was embedded and cut into 3 μ m paraffin sections. After the paraffin sections were dewaxed in water, they were stained with H&E and Masson's solution according to the manufacturer's instructions.

For TUNEL-stained sections, after paraffin sections were dewaxed in water, antigenic repair was performed with Proteinase K working solution, membrane disruption was performed with 0.5 % Triton X-100, and endogenous peroxidase activity was blocked with 3 % H₂O₂. Then, TUNEL staining was performed on the sections.

2.6.6. Transmission electron microscopy (TEM)

The left ventricular tissue of the rats was prefixed with 3 % glutaraldehyde, fixed with 1 % osmium tetroxide, progressively dehydrated with acetone, and embedded in Epon812. Semithin sections of left ventricular tissue were stained with methylene blue for optical localization. The sections were cut into ultrathin sections with a diamond knife. Uranyl acetate and lead citrate were used to stain the ultrathin sections. Finally, the sections were observed and imaged using a JEM-1400FLASH transmission electron microscope (Japan Electron Optics Laboratory, Tokyo, Japan).

2.7. Cell experiment

2.7.1. Effects of CHX on H9c2 cells

H9c2 cells were treated with CHX at concentrations of 6.25, 12.5, 25, 50, 100, 200 and 400 μ g/mL in 96-well plates. After incubation for 24 h, the cytotoxicity of CHX was detected by the CCK-8 method.

After detecting the cytotoxicity of CHX, we pretreated cells with CHX (6.25, 12.5, 25, 50 and 100 μ g/mL) for 12 h and then induced them with 80 μ g/mL ISO for 24 h to observe whether CHX had a protective effect on ISO-induced cell viability reduction.

2.7.2. Flow cytometry

H9c2 cells (1 \times 10⁵ cells/well) were inoculated in 6-well plates. We divided the cells into a normal group, an ISO group and CHX groups. In the CHX groups, the cells were pretreated with 25, 50, or 100 μ g/mL CHX and 80 μ g/mL ISO for 12 h or 24 h. The ISO group did not undergo CHX preprocessing but was treated with ISO. EDTA-free trypsin was used to collect the cells. The cells were washed with PBS, diluted to 1 \times 10⁶ cells/mL and resuspended in Annexin V binding buffer. Then, 100 μ L of cells were cultured with Annexin V-FITC and PI dyes. Finally, H9c2 cells were detected with a FACSCanto II flow cytometer (BD Company, New York, NY, USA).

After treatment with CHX and ISO, the 6-well plates were treated with DCFH-DA and JC-1 fluorescent probes for 30 min to detect reactive oxygen species (ROS) and the mitochondrial membrane potential (MMOP). Then, the staining solution was removed, and the cells were washed 3 times with PBS. Finally, the ROS and MMOP levels in H9c2 cells were detected by a FACSCanto II flow cytometer.

2.7.3. Immunofluorescence

H9c2 cells were seeded and treated in laser confocal plates as described above. PBS and paraformaldehyde were used to clean and incubate the cells. Then, the cells were infiltrated with 0.3 % Triton X-100 and incubated with 10 % serum for 1 h. The cells were incubated with primary antibodies against Dvl-1 (1:100), Bcl-2 (1:100), and Bax (1:200) overnight at 4 $^{\circ}$ C. The cells were then incubated with secondary antibodies (1:150) at room temperature for 2 h. Finally, fluorescent sealant was added to the cells after the cells were washed. The cells were immediately observed by laser confocal microscopy (Leica, SP8 SR, Wetzlar, Germany).

We used a DCFH-DA fluorescent probe to detect ROS and a JC-1 fluorescent probe to examine the MMOP intracellular content. Briefly, H9c2 cells (1 \times 10⁵ cells/well) were treated for 12 h with CHX (25, 50, or 100 μ g/mL) or for 24 h with ISO. Then, the culture medium was removed, and the cells were incubated with DCFH-DA and JC-1

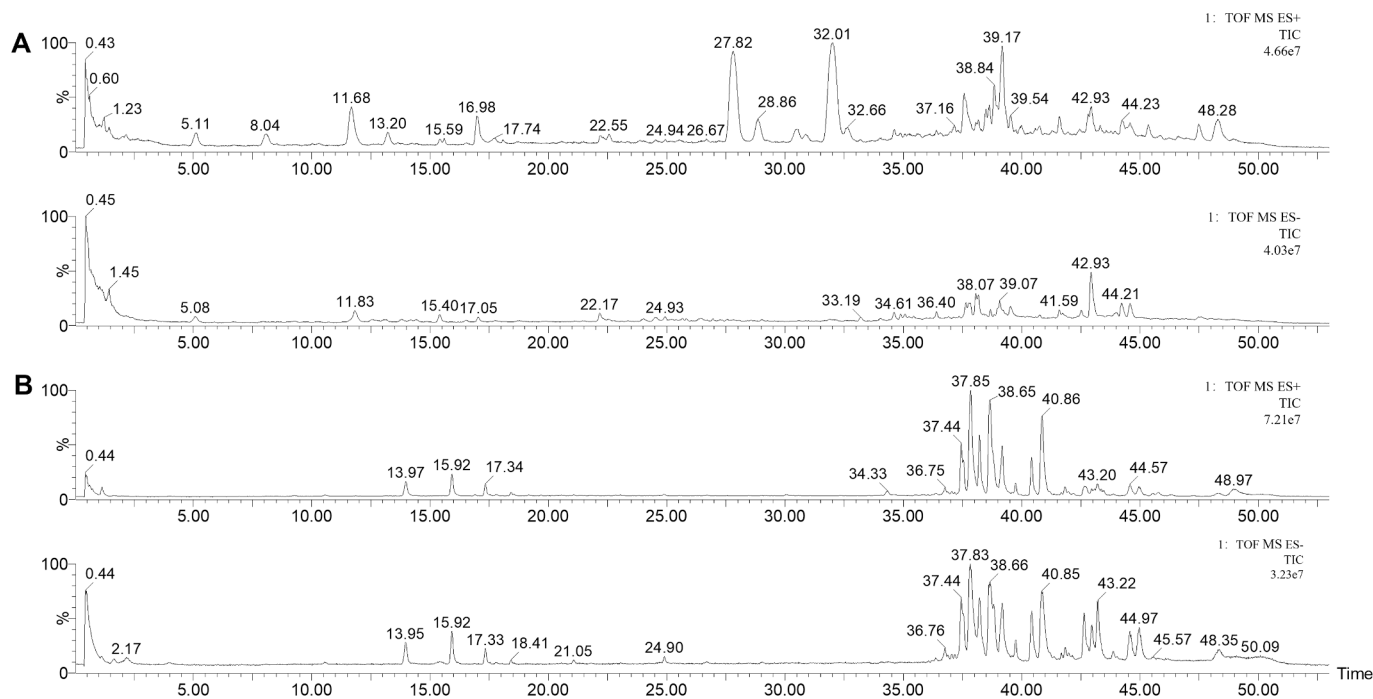


Fig. 1. TIC chromatograms of CHX extracts and blood samples. (A) TIC chromatograms of CHX extracts in positive (upper) and negative (lower) modes. (B) TIC chromatograms of blood samples in positive (upper) and negative (lower) modes.

fluorescent probes. The excess fluorescent probe was removed by washing with PBS. Laser confocal microscopy was used to detect and analyze the fluorescence intensity.

2.7.4. Cell SOD, MDA and GSH-PX levels

As described above, H9c2 cells were incubated with CHX and ISO in 6-well plates. We used PBS to wash the cells (1×10^5 cells/well) and collected total protein in RIPA buffer. Finally, following the manufacturer's instructions, we used commercial assay kits to determine the MDA, SOD and GSH-Px levels in the cells.

2.7.5. Western blot analysis

H9c2 cells (7×10^6) were cultured in petri dishes. After the cells were treated with CHX (100 $\mu\text{g}/\text{mL}$) and ISO, RIPA buffer was used to obtain total cell protein. For nuclear protein extraction, cells were collected using a cell scraper. Two hundred microliters of plasma protein extraction reagent containing PMSF was added to 2×10^6 cells, and the cells were swirled into a single-cell suspension. After centrifugation, the supernatant was removed, and 100 μL of nuclear protein extraction reagent was added to the precipitate. After vortexing in an ice bath, the supernatant was collected as the nuclear protein. Next, we used a BCA protein assay kit to determine the protein concentration and SDS-PAGE to isolate the prepared proteins. Then, the proteins were transferred to activated PVDF membranes. The PVDF membranes were incubated overnight with antibodies against C-Caspase-3 (1:1000), Caspase-3 (1:1000), Bcl-2 (1:1000), Bax (1:6000), Dvl-1 (1:1000), Nrf2 (1:1000), Akt (1:3000), p-Akt (1:1000), Wnt-1 (1:2500), Wnt-3 (1:1100), β -Catenin (1:300), GSK-3 β (1:1000), and p-GSK-3 β (1:500) at 4 $^\circ\text{C}$ and HRP-conjugated secondary antibodies (1:2000) for 1 h at room temperature. Finally, we visualized the protein bands with an enhanced chemiluminescence (ECL) kit. ImageJ software was used to analyze the grayscale value of each blot.

In our study, GAPDH (1:50,000) was selected as the internal reference for total cell protein (Lee et al., 2016). However, GAPDH is not expressed in the nucleus. Lamin B1 is a nuclear membrane structural component that is highly conserved between species and is often used as a reference in samples with a nuclear envelope. Therefore, we selected

Lamin B1 (1:1000) as the internal reference for nuclear protein.

2.7.6. Use of the Akt inhibitor MK-2206

To further verify the molecular mechanism of the anti-MI effect of CHX, cells were pretreated with the Akt inhibitor MK-2206 along with 25, 50, or 100 $\mu\text{g}/\text{mL}$ CHX for 12 h and then treated with ISO for 24 h. Images of the cells in the normal group, ISO model group and MK-2206 + CHX groups were observed and recorded under an optical microscope. Finally, an Annexin V-FITC/PI apoptosis detection kit was used to detect the percentage of apoptotic cells after the addition of MK-2206 by flow cytometry.

2.8. Statistical analysis

The data are presented as the means \pm standard deviations (means \pm SDs). IBM SPSS Statistics 26 software was used to test the normality of each set of data. One-way analysis of variance (ANOVA) was used when the data met the normal distribution, the least significant difference (LSD) test was selected when the variance was homogeneous, and the Dunnett T3 test was selected when the variance was not homogeneous. When the data did not conform to a normal distribution, the Kruskal-Wallis H test was used. In this paper, statistically significant differences are presented as $*p < 0.05$, highly significant differences are presented as $**p < 0.01$, and statistically nonsignificant differences are presented as $^{\&}p > 0.05$.

3. Results

3.1. Blood entry constituents of CHX and extraction process optimization

3.1.1. Blood entry constituents and their protective effects on H9c2 cells

The total positive/negative ion flow diagrams of CHX and CHX-containing serum are shown in Fig. 1A–1B. Table 1 shows the details of the CHX compounds. A total of 49 compounds were detected in the CHX extract. In negative ion mode, 24 compounds, such as caffeic acid, vanillic acid and ferulic acid, were obtained. A total of 25 compounds, such as butylphthalide, senkyunolide I and tetramethylpyrazine (TMP),

Table 1
UPLC-Q-TOF-MS/MS analysis of EtOH extracts of CHX roots.

No.	Name	MF	t _R (min)	[M + H] ⁺	[M-H] ⁻	MS/MS
1	Ferulic Acid	C ₁₀ H ₁₀ O ₄	5.16		193.0481	178.0297,149.0593,134.0374
2	Vanillic acid	C ₈ H ₈ O ₄	2.15		167.0368	123.0436
3	Caffeic acid	C ₉ H ₈ O ₄	0.46		179.0577	135.0294
4	Butylphthalide	C ₁₂ H ₁₄ O ₂	32.02	191.1088		173.0961,145.1025,117.0696
5	Z-Ligustilide	C ₁₂ H ₁₄ O ₂	32.38	191.1088		173.0961,145.1025,117.0696,105.0569
6	(Z)-6,7- epoxyLigustilide	C ₁₂ H ₁₄ O ₃	13.2	207.1052		189.0908,161.0957,133.0680
7	Senkyunolide A	C ₁₂ H ₁₆ O ₂	27.8	193.1277		193.1288,175.1156,147.1183, 137.062,119.0883,105.0712
8	Senkyunolide I	C ₁₂ H ₁₆ O ₄	11.68	225.1651		207.1065,189.0908,163.0756,119.0883
9	N-Butylidenephthalide	C ₁₂ H ₁₂ O ₂	13.21	189.0908		189.0908,161.1002,133.0680,105.0712
10	4-Hydroxy-3-Butylphthalide	C ₁₂ H ₁₄ O ₃	13.20	207.1065		189.0908,165.0585,161.0957, 133.0680,105.0712
11	Palmitic acid	C ₁₆ H ₃₂ O ₂	44.20		255.2322	255.2322
12	Levistilide A	C ₂₄ H ₂₈ O ₄	39.19	381.2016		191.1088
13	(E)-6,7-transdihydroxyLigustilide	C ₁₂ H ₁₆ O ₄	37.49	255.1651		207.1065,189.0908,105.0712
14	Xanthoxol	C ₁₁ H ₆ O ₄	37.98	203.1809		175.0783,147.1183
15	Isopimpinellin	C ₁₃ H ₁₀ O ₅	11.67	247.0908		189.0908,161.0957,133.0680,105.0712
16	Tetramethylpyrazine	C ₈ H ₁₂ N ₂	1.99		135.0457	
17	Chlorogenic acid	C ₁₆ H ₁₈ O ₉	11.86		353.0899	191.0534
18	3-Hydroxyquinoline	C ₉ H ₇ NO	1.22		146.0619	118.0653,115.0569
19	Quinic acid	C ₇ H ₁₂ O ₆	0.50		191.0583	179.0577,161.0467
20	L-Pyroglutamic acid	C ₅ H ₇ NO ₃	0.60		128.0353	119.0364
21	Piperonylic acid	C ₈ H ₆ O ₄	2.01		165.0189	121.0298
22	E-Butylidenephthalide	C ₁₂ H ₁₂ O ₂	32.65	189.0908		171.0837,161.0600
23	3,5-Isochlorogenic acid B	C ₂₅ H ₂₄ O ₁₂	1.05		515.1190	353.0899,191.0583,179.0530
24	Comiferyl ferulate	C ₂₀ H ₂₀ O ₆	22.14		355.1163	193.0530
25	Senkyunolide G	C ₁₂ H ₁₆ O ₃	8.08	209.1215		191.1088, 163.1115
26	Senkyunolide F	C ₁₂ H ₁₄ O ₃	22.32		205.0878	161.0958
27	Senkyunolide M	C ₁₆ H ₂₂ O ₄	26.65	279.1587		261.0906,233.1540
28	3-Butylidene-7-hydroxyphthalide	C ₁₂ H ₁₂ O ₃	26.43		203.0718	173.0251,160.0167,145.0308,132.0201
29	Senkyunolide E	C ₁₂ H ₁₂ O ₃	28.03		203.0718	159.0832
30	Cnidium lactone	C ₁₂ H ₁₈ O ₂	30.84	195.1376		177.0578,149.1352
31	RiLigustilide	C ₂₄ H ₂₈ O ₄	37.57	381.2061		213.0884, 191.1088
32	Senkyunolide P	C ₂₄ H ₃₀ O ₄	38.49	383.2215		191.1088
33	Neochlorogenic acid	C ₁₆ H ₁₈ O ₉	1.44	355.1047		163.0397,145.0304,135.0437
34	3-butyl-3,6,7-trihydroxy-4,5,6,7-tetrahydrophthalin	C ₁₂ H ₁₈ O ₅	25.53	243.0780		225.0912,207.1014
35	Isochlorogenic Acid B	C ₂₅ H ₂₄ O ₁₂	11.84		515.1163	353.0899,191.0534,179.0342,135.0457
36	Progesterone	C ₂₁ H ₃₀ O ₂	34.49	315.2314		
37	Chuangxiangnolide A	C ₂₄ H ₂₈ O ₅	34.78	397.2046		
38	Wallichilide	C ₂₅ H ₃₂ O ₅	38.88	413.2315		
39	2-Methoxy-4-vinylphenol	C ₉ H ₁₀ O ₂	11.39		149.0249	
40	Vinylphenol	C ₈ H ₈ O ₄	11.39		167.0368	
41	Senkyunolide R	C ₁₂ H ₁₆ O ₅	6.82		239.0953	
42	Linoleic acid	C ₁₈ H ₃₂ O ₂	42.92		279.2335	
43	3-n-butyl-4-hydroxyphthalide	C ₁₂ H ₁₄ O ₃	24.03		205.0878	
44	Senkyunolide H	C ₁₂ H ₁₆ O ₄	11.59	247.0989 [M + Na] ⁺		207.1014
45	Caffeoylquinic acids	C ₁₆ H ₁₈ O ₉	1.45		353.0899	
46	Senkyunolide J	C ₁₂ H ₁₈ O ₄	8.09	475.2326 [M + Na] ⁺		249.1106
47	Senkyunolide D	C ₁₂ H ₁₄ O ₄	19.80		221.0822	
48	Sedanolide	C ₁₂ H ₁₈ O ₂	31.82	195.1376		
49	3, 6-Dihydroxy-p	C ₁₁ H ₁₄ O ₃	13.81		193.0873	

Table 2
Blood entry constituents of CHX extracts by UPLC-Q-TOF-MS/MS.

No.	Name	Rt (min)	MF	[M + H] ⁺	[M-H] ⁻	MS/MS
1	N-Butylidenephthalide	3.95	C ₁₂ H ₁₂ O ₂		187.0068	107.0514
2	Senkyunolide H	11.69	C ₁₂ H ₁₆ O ₄	247.0989 [M + Na] ⁺		207.1014
3	Senkyunolide I	11.84	C ₁₂ H ₁₆ O ₄	207.1014		189.0908,165.0585, 119.0883,105.0712
4	Senkyunolide A	42.64	C ₁₂ H ₁₆ O ₂	193.1227		175.1481,147.1183
5	Ferulic acid	44.95	C ₁₀ H ₁₀ O ₄	195.1769		177.1514
6	Butylphthalide	45.15	C ₁₂ H ₁₄ O ₂	191.1088		173.1331,145.1025
7	Ligustilide	45.54	C ₁₂ H ₁₄ O ₂	191.1088		145.1025,173.1311

were obtained in positive mode. Seven kinds of components were analyzed from CHX-containing serum: ferulic acid, ligustilide, senkyunolide I, senkyunolide H, butylphthalide, senkyunolide A, and N-butylidenephthalide (Table 2).

ISO induction in H9c2 cells can cause cell damage and oxidative

stress and increase the levels of inflammatory factors and the rate of apoptosis (Yang et al., 2022). As shown in Fig. 2A, when the ISO concentration was 80 µg/mL, the inhibition rate of H9c2 cells was 50 %. Therefore, in subsequent experiments, 80 µg/mL ISO was selected as the modeling concentration for the cell experiments.

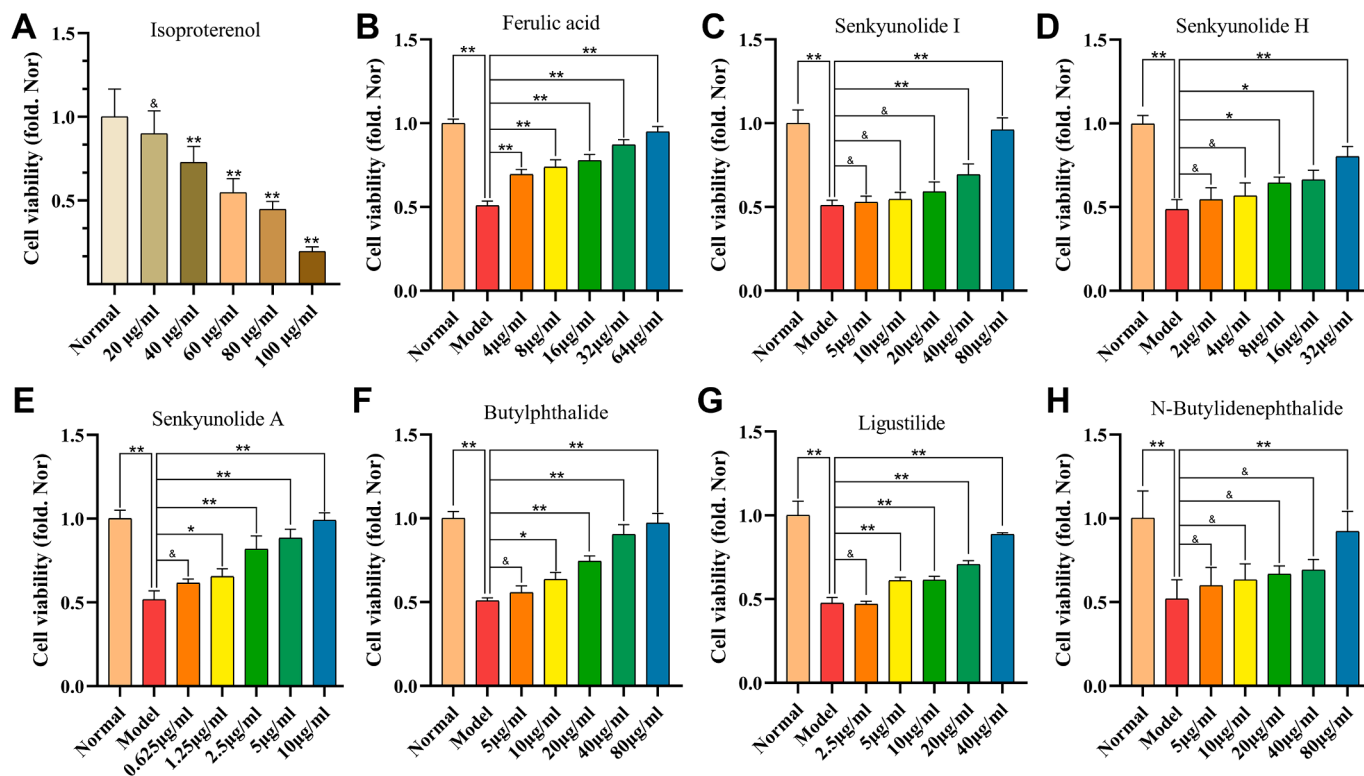


Fig. 2. Protective effects of the active compounds in CHX against cardiomyocytes. (A) The impact of ISO on cell viability. (B)–(H) Protective effects of active compounds in CHX against cardiomyocytes according to CCK-8 assays. B–H represent ferulic acid (B), senkyunolide I (C), senkyunolide H (D), senkyunolide A (E), butylphthalide (F), ligustilide (G), and N-butylidenephthalide (H), respectively. The data are expressed as the means \pm SDs ($n = 3$). * $p < 0.05$, ** $p < 0.01$, $\#p > 0.05$ vs. the Model group.

Table 3

Factors and levels of the orthogonal design and experimental results.

No.	Factor				Overall score
	A: Extraction time (h)	B: Solid-liquid ratio	C: EtOH Conc. (%)	D: Extraction times	
1	1.5	1:10	40	1	0.375
2	1.5	1:15	60	2	1.019
3	1.5	1:20	80	3	4.413
4	2	1:10	60	3	0.479
5	2	1:15	80	1	0.309
6	2	1:20	40	2	0.357
7	2.5	1:10	80	2	0.511
8	2.5	1:15	40	3	0.387
9	2.5	1:20	60	1	0.393
K1	1.935	0.359	0.373	0.455	
K2	0.382	0.629	0.630	0.572	
K3	0.430	1.759	1.744	1.721	
R	1.554	1.401	1.372	1.266	

Fig. 2B–2H shows that all 7 blood entry constituents of CHX had protective effects on ISO-treated H9c2 cells. Therefore, we used these 7 components as quality markers (Q-markers) of CHX to optimize the extraction method of CHX.

3.1.2. Optimized CHX extraction process

The relative standard deviations (RSDs) for the methodological verification of instrument precision, method repeatability and sample stability were all less than 2%. The Q-marker linear regression equations are shown in Table S3, Supporting Information. The recovery rates of ferulic acid, senkyunolide A, senkyunolide I, ligustilide, senkyunolide H, N-butylidenephthalide, and butylphthalide were 93.96%, 94.70%, 94.53%, 92.75%, 95.58%, 99.05% and 94.60%, respectively.

According to the AHP method, the weight coefficients of ferulic acid,

senkyunolide I, senkyunolide H, senkyunolide A, butylphthalide, ligustilide and N-butylidenephthalide were 0.3517, 0.1040, 0.0678, 0.1596, 0.0449, 0.2412 and 0.0308, respectively. The consistency scaling factor (CR) = 0.03 < 0.1 conformed to the consistency test, indicating that the weight coefficient was valid. Overall score = 0.3517* content of ferulic acid + 0.1040* content of senkyunolide I + 0.0678* content of senkyunolide H + 0.1596* content of senkyunolide A + 0.0449* content of butylphthalide + 0.2412* content of ligustilide + 0.0308* content of N-butylidenephthalide.

The results of the range analysis of the orthogonal experiments are shown in Table 3. According to our analysis, the influence sequence of each factor was A > B > C > D, and the optimal extraction process was A₁B₃C₃D₃. That is, the extraction time was 1.5 h, the solid-liquid ratio was 1:20, the EtOH concentration was 80%, and the number of extractions was 3.

3.2. Protective effect of CHX on MI rats

3.2.1. CHX protects heart integrity and function

ECG showed that rats in the MI group 1 h after intraperitoneal injection of ISO exhibited ST segment elevation (Fig. 3A), while no phenomenon was observed in the Dil and CHX (600, 900, 1200 mg/mL) groups. These findings indicate the success of the ISO-induced MI model and the inhibitory effect of CHX on MI. This finding was further demonstrated by echocardiography, which revealed that CHX and Dil can increase ISO-induced fractional shortening (FS) and decrease the ejection fraction (EF) (Fig. 3B–3D).

Rats pretreated with CHX had lower serum cTnT, LDH and CK-MB levels than rats in the MI group (Fig. 3E–3G). Compared with those in the normal group, the cardiac indices of the rats in the MI group were significantly greater ($p < 0.05$). However, neither Dil nor CHX significantly affected the reduction in the cardiac indices ($p > 0.05$) (Fig. 3H).

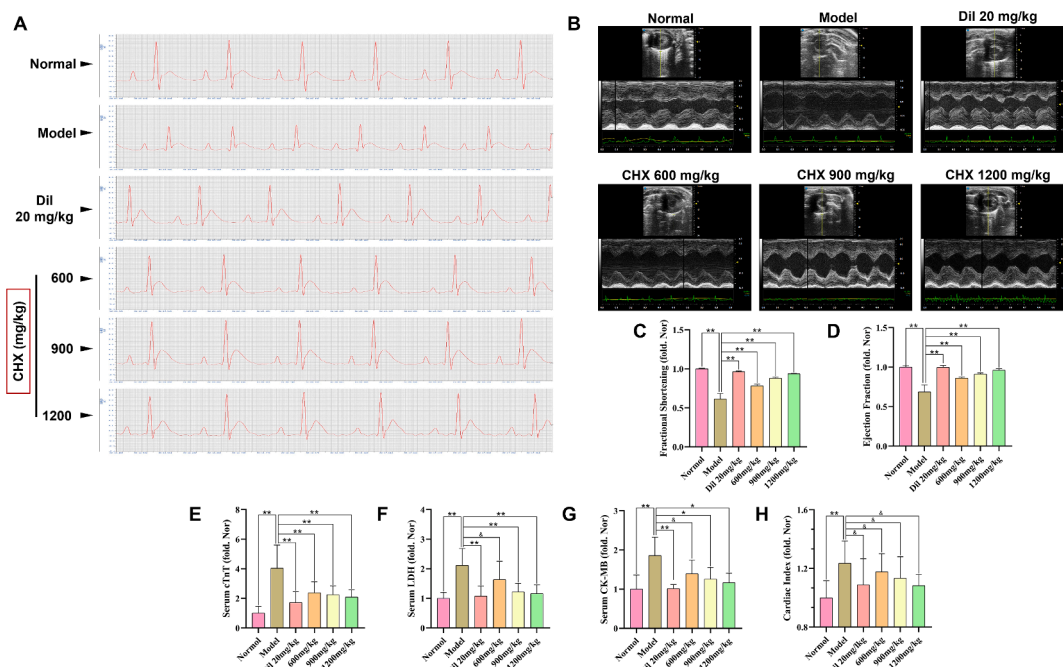


Fig. 3. Effects of CHX on ISO-induced myocardial injury in MI rats. (A) Rat electrocardiogram detection. (B) M-mode echocardiography. (C) Rat fractional shortening. (D) Rat ejection fraction. (E) Serum cTnT levels. (F) Serum LDH levels. (G) Serum CK-MB levels. (H) Rat heart index. The data are expressed as the means \pm SDs (n = 6). * p < 0.05, ** p < 0.01, & p > 0.05 vs. the Model group.

3.2.2. H&E and Masson staining

The most common method for clinicopathological diagnosis is H&E staining (Varasteh et al., 2019). In our study, H&E staining revealed that compared with those of normal rats, the myocardial fibers of the left ventricular heart tissue of MI rats were denatured or broken. Intercellular collagen fibers were significantly increased. Myocardial cells were necrotic. The heart tissues were infiltrated by inflammatory cells. In the Dil group, myocardial fibrosis or rupture was observed in the rats. In the CHX 600 mg/mL group, cardiomyocyte necrosis, inflammatory cell infiltration and myocardial fiber shrinkage were observed. In the CHX 900 mg/mL group, myocardial fibroblast proliferation was observed. In the CHX 1200 mg/mL group, inflammatory cell infiltration was observed (Fig. 4A).

The heart, liver, spleen, kidney, and lung tissues of the normal group and the 1200 mg/kg CHX group were stained with H&E to determine whether CHX was toxic to the internal organs of the rats. The results (Fig. S3, Supporting Information) showed that CHX had no toxic effect on rat organs.

The principle of Masson staining is related to the size of anionic dye molecules and the degree of tissue penetration. The macromolecule aniline blue can only enter loose structures and high-permeability collagen fiber tissue to appear blue. Ponceau combines with muscle fibers to form red fibers. Therefore, Masson's trichrome staining can be used to observe organ fibrosis (Hao and Jiao, 2022). Masson staining showed that ISO increased the amount of collagen fibers in the hearts of the rats. CHX and Dil reduced the increase in collagen fibers and prevented cardiac fibrosis (Fig. 4B).

3.2.3. Heart TEM and TUNEL oxidative stress assays

TEM revealed mitochondrial swelling, myoplasmic reticulum expansion, myofibrillar dissolution and lipid drop formation in the heart tissue of the MI group. However, 1200 mg/mL CHX prevented these changes (Fig. 5A). Immunohistochemical TUNEL results showed that myocardial cell apoptosis occurred in the MI group rats. CHX and Dil reduced ISO-induced cardiomyocyte apoptosis (Fig. 5B–5C). MDA, SOD and GSH-Px in the serum and heart tissue of the rats were detected (Fig. 5D–5I). An increase in the content of MDA and decreases in the

activity of SOD and GSH-Px were detected in the MI group. However, after ISO induction, CHX and Dil decreased the MDA content and upregulated the activity of GSH-Px and SOD in serum and heart tissue.

3.3. CHX protects H9c2 cells

3.3.1. CHX prevents ISO-induced apoptosis

The CCK-8 assay results showed that concentrations of 6.25, 12.5, 25, 50, and 100 μ g/mL CHX extract were not toxic to H9c2 cells (p > 0.05). However, CHX concentrations of 200 and 400 μ g/mL decreased cell viability (Fig. 6A). CHX at concentrations of 25, 50, and 100 μ g/mL protected ISO-induced H9c2 cells (p < 0.01) (Fig. 6B). Flow cytometry showed that ISO induced cell apoptosis, while CHX pretreatment reduced the apoptosis rate (Fig. 6C–6D).

We further detected the expression of apoptosis-related proteins by immunofluorescence. As shown in Fig. 6E–6F, Bcl-2 is represented by red fluorescence, and Bax is represented by green fluorescence. By determining the fluorescence intensity of Bax and Bcl-2, the Bax/Bcl-2 ratio was calculated, and the relative expression levels of the two proteins were determined. The results showed that ISO increased the Bax/Bcl-2 ratio, while different concentrations of CHX decreased the Bax/Bcl-2 ratio.

3.3.2. CHX protects against ISO-induced MMOP reduction

JC-1 is an ideal MMOP fluorescent probe. A change in JC-1 from red to green fluorescence is an early indicator of apoptosis. In our study, the red fluorescence intensity of H9c2 cells decreased sharply after ISO treatment, as did the ratio of red to green fluorescence (p < 0.01). However, CHX increased the MMOP of the cells (Fig. 7A–7B). Flow cytometry analyses of MMOP are shown in Fig. 7C, where red cell clusters represent cells with normal MMOP and green cell clusters in the rectangular box represent cells with decreased MMOP. The statistical results showed that the effect of ISO on MMOP reduction can be prevented by CHX (Fig. 7D).

3.3.3. CHX reduces ISO-induced cellular oxidative stress

GSH-Px, MDA and SOD in total cell protein were detected by a

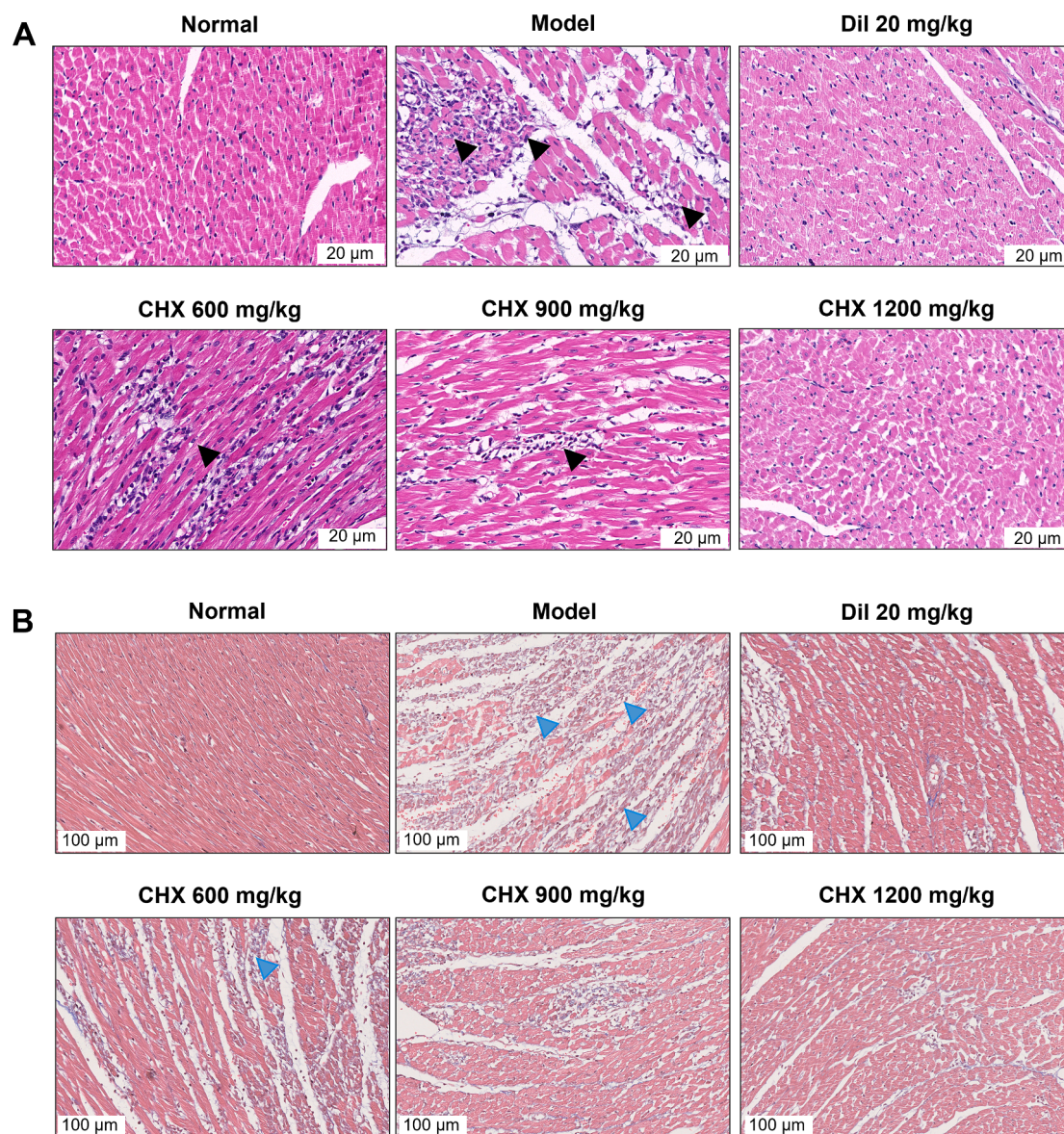


Fig. 4. Effects of CHX on myocardial pathological injury in MI rats. (A) Representative images of H&E staining; black arrows show the location of myocardial injury. (B) Representative images of Masson staining; blue arrows show collagen deposition. (For interpretation of the references to color in this figure legend, the reader is referred to the web version of this article.)

commercial kit. ISO increased the MDA content and decreased the activities of GSH-Px and SOD in cells. However, 50 and 100 $\mu\text{g}/\text{mL}$ CHX increased the activity of GSH-Px and SOD. CHX (25, 50 and 100 $\mu\text{g}/\text{mL}$) decreased the MDA concentration (Fig. 8A–8C). Intracellular ROS levels were measured by flow cytometry and immunofluorescence. DCFH-DA is a cellular permeability indicator of ROS, and in a nonoxidizing environment, it has no fluorescence. In an oxidizing environment, DCFH-DA transforms into 2,7-dichlorodihydrofluorescein, which emits green fluorescence. According to the statistical analysis of fluorescence intensity, ISO increased the level of ROS in cells, while CHX reduced the level of ROS (Fig. 8D–8G).

3.3.4. Effect of CHX on the Dvl-1/Akt/GSK-3 β /Nrf2 signaling pathway

Immunofluorescence results (Fig. 9A–9B) demonstrated that CHX promoted Dvl-1 protein expression. With GAPDH as the extracellular reference and Lamin B1 as the intracellular reference, the western blot results showed that CHX can increase the phosphorylation of Akt and GSK-3 β , promote Nrf2 entry into the nucleus, and inhibit the cleavage of Caspase-3. In addition, the Bax/Bcl-2 ratio decreased, and the

expression levels of β -catenin, Wnt-3 and Dvl-1 increased in response to CHX. However, CHX had no effect on Wnt-1 (Fig. 9C–9M).

3.3.5. MK-2206 inhibits the anti-Mi effect of CHX

As shown in Fig. 10A, cell damage increased in the CHX groups after the addition of the Akt inhibitor MK-2206. Flow cytometry was used to measure apoptosis after adding MK-2206, and MK-2206 increased the percentage of apoptotic cells in the CHX groups (Fig. 10B–10C). These two studies showed that the protective effect of CHX on H9c2 cells was reversed by MK-2206.

4. Discussion

Oral medications need to pass through the digestive system and into the bloodstream first. Then, drugs are transported to various tissues, organs, tissue spaces and cells in the blood circulation, bind to receptors, and affect or change information transmission in the body to play a therapeutic role (Koziolek et al., 2019). The multicomponent characteristics of TCM make it difficult to define the material basis of its

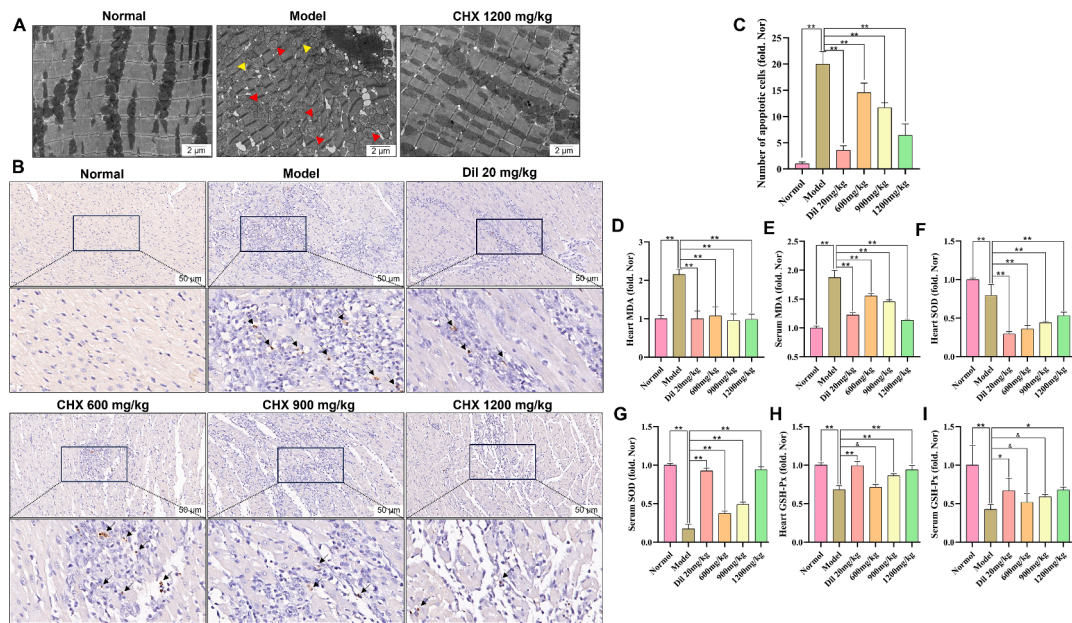


Fig. 5. Effects of CHX on myocardial ultrastructure, apoptosis, and oxidative stress in MI rats. (A) Images of the ultrastructure of the rat myocardium observed by transmission electron microscopy. The yellow arrows represent myofibrillar dissolution, and the red arrows represent mitochondrial swelling. (B)–(C) The results of TUNEL staining; the black arrows represent apoptotic cells. (D)–(E) MDA levels in the serum and heart tissues of MI rats. (F)–(G) SOD activity in the serum and heart tissues of MI rats. (H)–(I) GSH-Px activity in the serum and heart tissues of MI rats. The data are expressed as the means \pm SDs ($n = 6$). * $p < 0.05$, ** $p < 0.01$, & $p > 0.05$ vs. the Model group. (For interpretation of the references to color in this figure legend, the reader is referred to the web version of this article.)

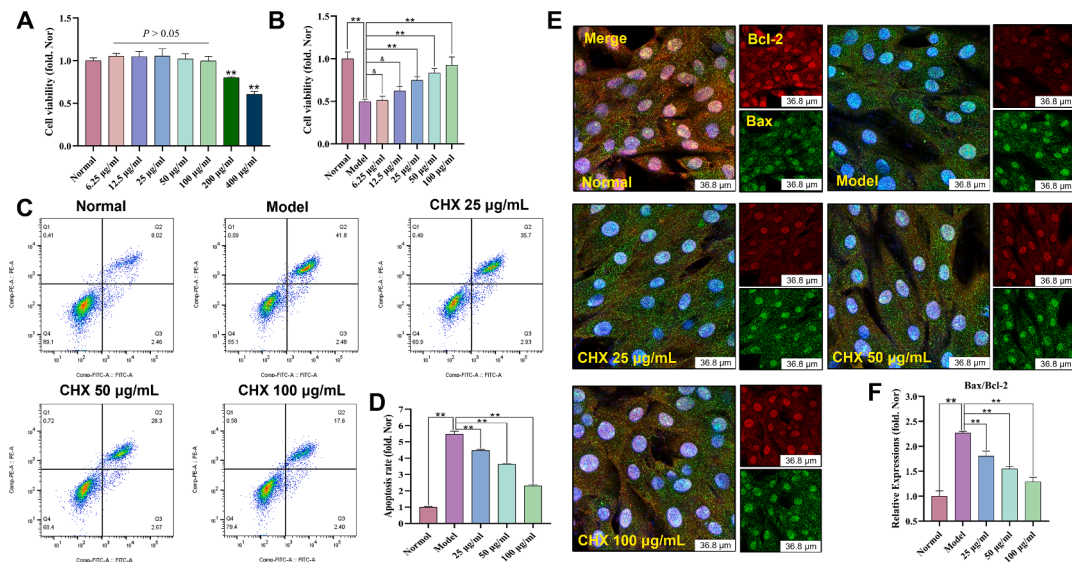


Fig. 6. Effects of ISO-induced CHX on H9c2 cells. (A) Effects of CHX at various concentrations on H9c2 cells. (B) Effects of CHX on ISO-stimulated H9c2 cells. (C)–(D) Effects of CHX on the apoptosis of ISO-stimulated H9c2 cells. (E)–(F) Effects of CHX on the Bax/Bcl-2 ratio of ISO-stimulated H9c2 cells. The data are expressed as the means \pm SDs ($n = 3$). ** $p < 0.01$, & $p > 0.05$ vs. the Model group.

therapeutic effect. In our study, UPLC-Q-TOF-MS/MS analysis was performed on total CHX extract and drug-containing serum, and seven components of CHX were found to enter the blood. These components included ferulic acid, senkyunolide H, senkyunolide I, butylphthalide, senkyunolide A, N-butylidenephthalide and ligustilide. These seven ingredients have been studied for the treatment of cardiovascular disease. Ferulic acid can alleviate myocardial ischemia/reperfusion injury by upregulating AMPK α 2 expression and inhibiting ferroptosis (Liu et al., 2021). The synergistic effect of senkyunolide I and cryptotanshinone can downregulate the expression of coagulation factor II and suppress the formation of thrombi induced by phenylhydrazine in zebrafish (Li et al.,

2021b). Senkyunolide A can promote endothelium-dependent vascular relaxation through the eNOS-NO-sGC-GMP pathway and can induce concentration-dependent vasodilation of the coronary artery ring (Li et al., 2023). Butylphthalide can inhibit inflammation, oxidative stress and cardiomyocyte apoptosis after acute myocardial infarction (Bai et al., 2019). Liu et al. demonstrated that ferulic acid and ligustilide are effective components of CHX that play a protective role against MI in dogs (Liu et al., 2016). N-butylidenephthalide can reduce cardiac fibrosis in the chronic myocardial infarction stage (Lin et al., 2019). Our findings of the protective effects of these 7 components on ISO-induced H9c2 cells suggest that these 7 components are the active ingredients

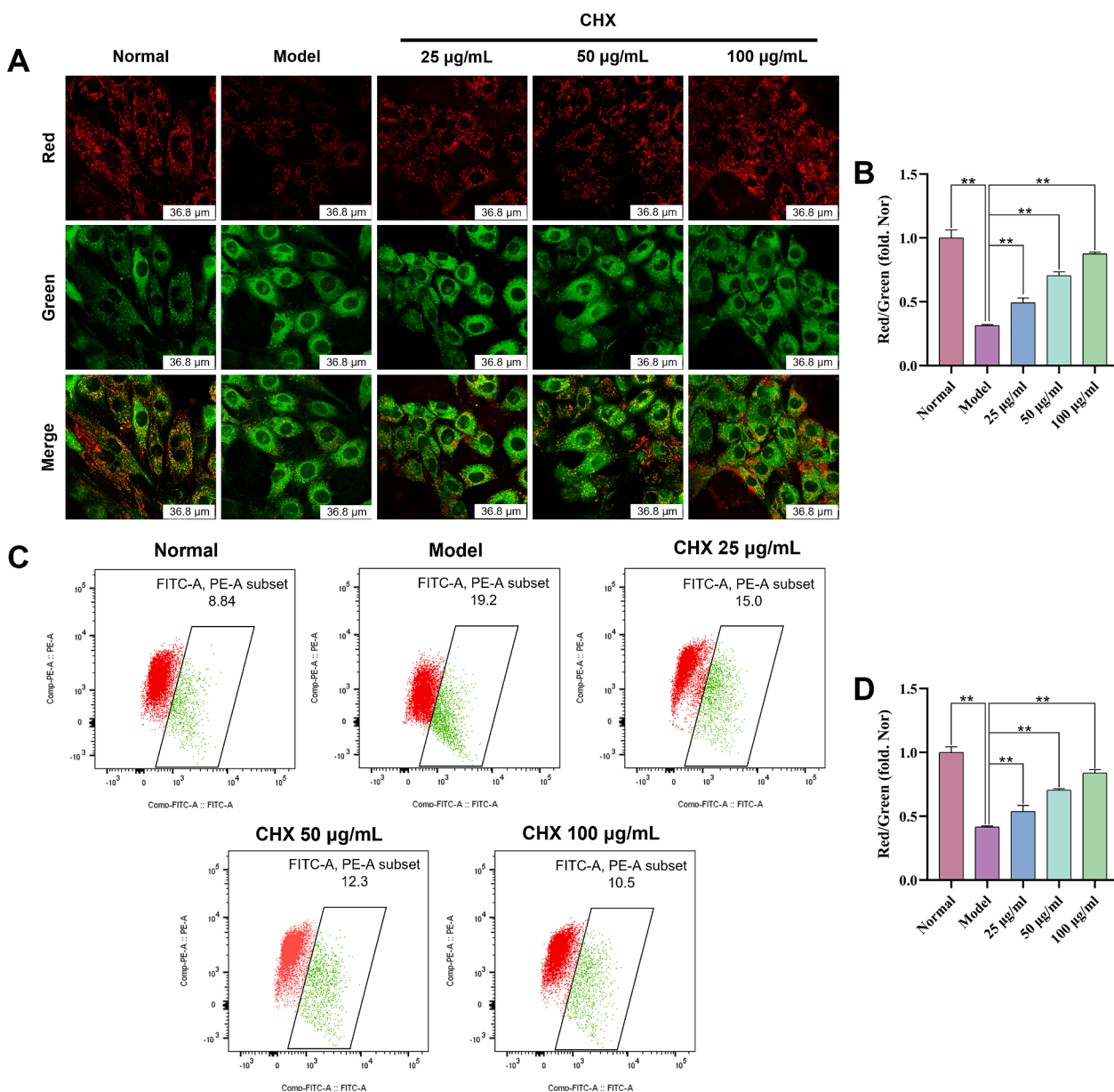


Fig. 7. Effects of CHX on the MMOP of ISO-treated H9c2 cells via confocal microscopy (A)–(B) and flow cytometry analysis (C)–(D). The data are expressed as the means \pm SDs ($n = 3$). $**p < 0.01$ vs. the Model group.

involved in CHX treatment of MI. Therefore, we consider these 7 components to be Q-markers of CHX and clarify the material basis of CHX treatment for MI.

Next, we used the Q-markers as indices to optimize the extraction process of CHX to maximize its therapeutic effect. Orthogonal experiments are advantageous in that they require less test time, produce good effects, involve simple methods and are highly efficient. Through a literature review and analysis of the Q-marker content in CHX, the weight coefficients of the Q-markers were determined by an analytic hierarchy process, and the overall score was calculated to evaluate the extraction rate of CHX. The optimal extraction conditions for single-factor and orthogonal experiments were as follows: an extraction time of 1.5 h, a solid–liquid ratio of 1:20, an EtOH concentration of 80 %, and 3 extractions.

ISO is a synthetic catecholamine and β -adrenergic agonist. Excessive intake of ISO causes irreversible damage to myocardial infarction in rats, resulting in an ECG similar to that observed in human myocardial infarction (Wang et al., 2020). Therefore, we selected rats for

intraperitoneal injection of ISO to establish an MI model. Dil is a non-dihydropyridine calcium channel blocker that is mainly used to treat angina pectoris, hypertension and myocardial infarction (Sen et al., 2021). Thus, it was used as a positive control drug. The principle of ECG is that the electrode generates a heart current, and then, the heart current is measured and displayed (Beck et al., 2021). The typical ECG feature of ischemic heart disease is ST segment elevation. This finding is consistent with what was observed in our MI group. This indicates that the ISO-induced MI model is valid. Treatment with CHX or Dil can change the ST segment elevation induced by ISO. High doses of ISO can also cause changes in heart morphology and function (Sun et al., 2018). Decreased EF is an important manifestation of MI and can lead to heart failure (Pagliaro et al., 2020). By examining the left ventricular wave group M pattern images, we found that ISO reduced the EF and FS of the left ventricle. Dil and CHX can increase the EF and FS. These results indicated that CHX could protect cardiac function in MI rats. Moreover, ISO can cause myocardial cell damage and loss of cell membrane functional integrity, thereby stimulating the release of cardiac marker

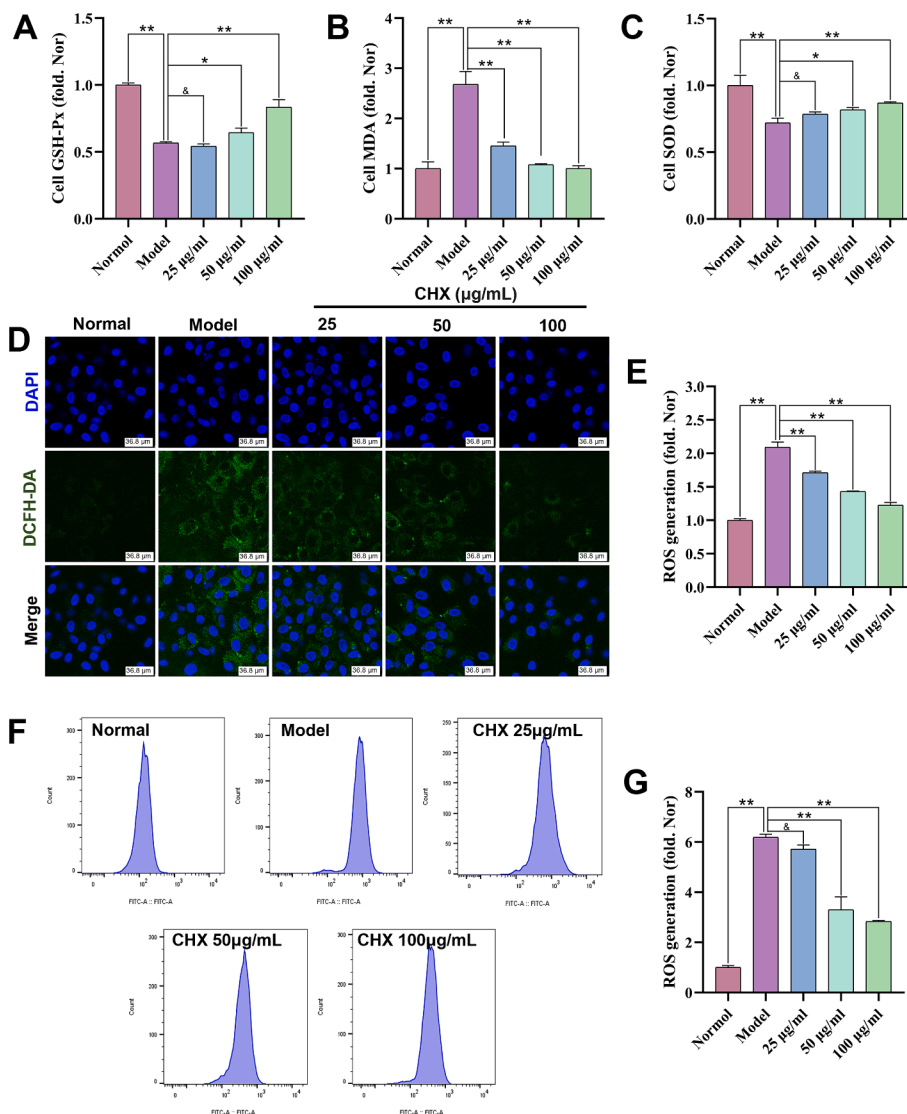


Fig. 8. Effects of CHX on oxidative stress levels in ISO-treated H9c2 cells. (A)–(C) Effects of CHX on GSH-Px, MDA, and SOD in ISO-treated H9c2 cells. (D)–(E) ROS levels determined via confocal microscopy. (F)–(G) Flow cytometry analysis. The data are expressed as the means \pm SDs ($n = 3$). * $p < 0.05$, ** $p < 0.01$, $\& p > 0.05$ vs. the Model group.

enzymes into the blood (Li et al., 2022). CHX can reduce the levels of serum cardiac marker enzymes, suggesting that CHX can protect cardiomyocyte integrity. ISO treatment can also cause pathological cardiac hypertrophy with cardiomyocyte dilation and ventricular thickening (Xing et al., 2022). We found that ISO can lead to an increase in the cardiac index, but CHX and Dil did not significantly reduce the cardiac index in MI rats. Cardiac injury is often accompanied by mitochondrial swelling (Bai et al., 2021), muscle fiber lysis and inflammation (Pacholewicz et al., 2019). H&E, TEM and Masson staining showed that CHX can reduce myocardial fibrosis and mitochondrial swelling and prevent myocardial inflammation and cell necrosis. CHX improved the histopathology findings in MI rats. ISO can stimulate oxidative stress in the rat heart, increase ROS levels in cells, destroy the MMOP, and cause cell apoptosis (Ni et al., 2021). Our study demonstrated that CHX can enhance the activities of GSH-Px and SOD in myocardial tissue and serum and reduce the MDA content and apoptosis rate in MI rats. The same phenomenon was observed in ISO-treated H9c2 cells. In addition, CHX can protect the MMOP and reduce ROS levels in cells. These findings suggested that CHX could protect ISO-induced MI rats and H9c2 cells by preventing oxidative stress and apoptosis.

Finally, we explored the molecular mechanism of the effect of CHX

treatment on MI in an ISO-induced H9c2 cell model. Nrf2 and Akt are important proteins that regulate oxidative stress and apoptosis. Akt regulates Nrf2 expression through its downstream molecule GSK-3 β . Nrf2 can promote the expression of cellular antioxidants and eliminate ROS (Mei et al., 2022). In our experiments, Akt and GSK-3 β in ISO-treated H9c2 cells were phosphorylated by CHX. CHX promoted the nuclear translocation of Nrf2. When CHX is used in conjunction with AKT inhibitor MK-2206, its cellular protective effect is inhibited. In the Wnt pathway, which is involved in heart damage repair, Axin, GSK-3 β , adenomatous polyposis coli, and casein kinase 1 α can bind to destructive complexes to phosphorylate and decompose β -catenin (Fu et al., 2019). The polymers formed by Dvl combined with Axin destroy destructive complexes and promote the incorporation of β -catenin into the nucleus. Once in the nucleus, β -catenin interacts with T-cell factor/lymphoid enhancing factor to activate the transcription of target genes downstream of Wnt (Nusse and Clevers, 2017). Our study showed that CHX can activate Dvl-1 and stimulate the expression of Wnt-3 and β -catenin. These results suggest that CHX protects ISO-treated H9c2 cells by activating the Dvl-1/Akt/GSK-3 β /Nrf2 signaling pathway. Among the proteins involved in controlling apoptosis, Caspase-3 and Bax can promote apoptosis, while Bcl-2 can inhibit apoptosis (Liu, 2018). Our research

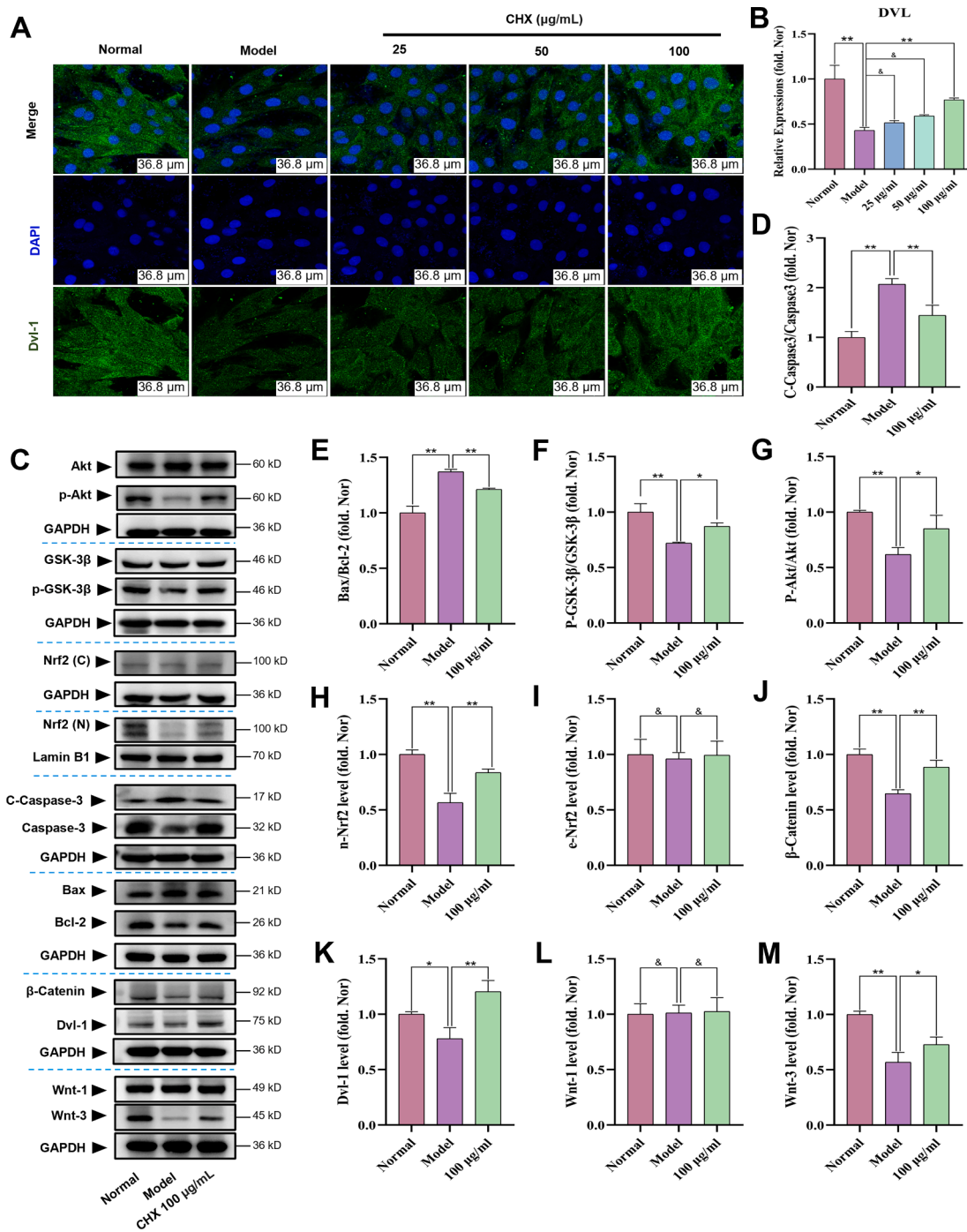


Fig. 9. Effects of CHX on Dvl-1/Akt/Nrf2 signaling in ISO-treated H9c2 cells. (A)–(B) Effects of CHX on Dvl-1 in ISO-treated H9c2 cells as determined by confocal microscopy. (C)–(M) Effects of CHX on Dvl-1/Akt/Nrf2 signaling in ISO-treated H9c2 cells as determined by western blotting. The data are expressed as the means ± SDs (n = 3). **p* < 0.05, ***p* < 0.01, &*p* > 0.05 vs. the Model group.

showed that the antiapoptotic effect of CHX was related to a reduction in C-Caspase-3 expression and the Bax/Bcl-2 ratio. This study of the molecular mechanism of CHX in the treatment of MI provides a pharmaceutical research basis for the development of new drugs for CHX and provides a scientific basis for the clinical application of CHX in the treatment of MI diseases.

5. Conclusion

In general, we analyzed the blood entry constituents of CHX and observed the protective effects of the constituents on H9c2 cells to

confirm their utility as Q-markers of CHX. We optimized the extraction process of CHX based on the Q-markers. In vivo and in vitro MI models were established by ISO, and CHX was shown to have a cardioprotective effect on MI rats. The mechanisms underlying the anti-MI effects of CHX are interrelated with its antioxidative stress and antiapoptotic effects. The mechanism of action involves the activation of the Dvl-1/Akt/GSK-3β/Nrf2 pathways by CHX.

Funding

This work was supported by the Sichuan Science and Technology

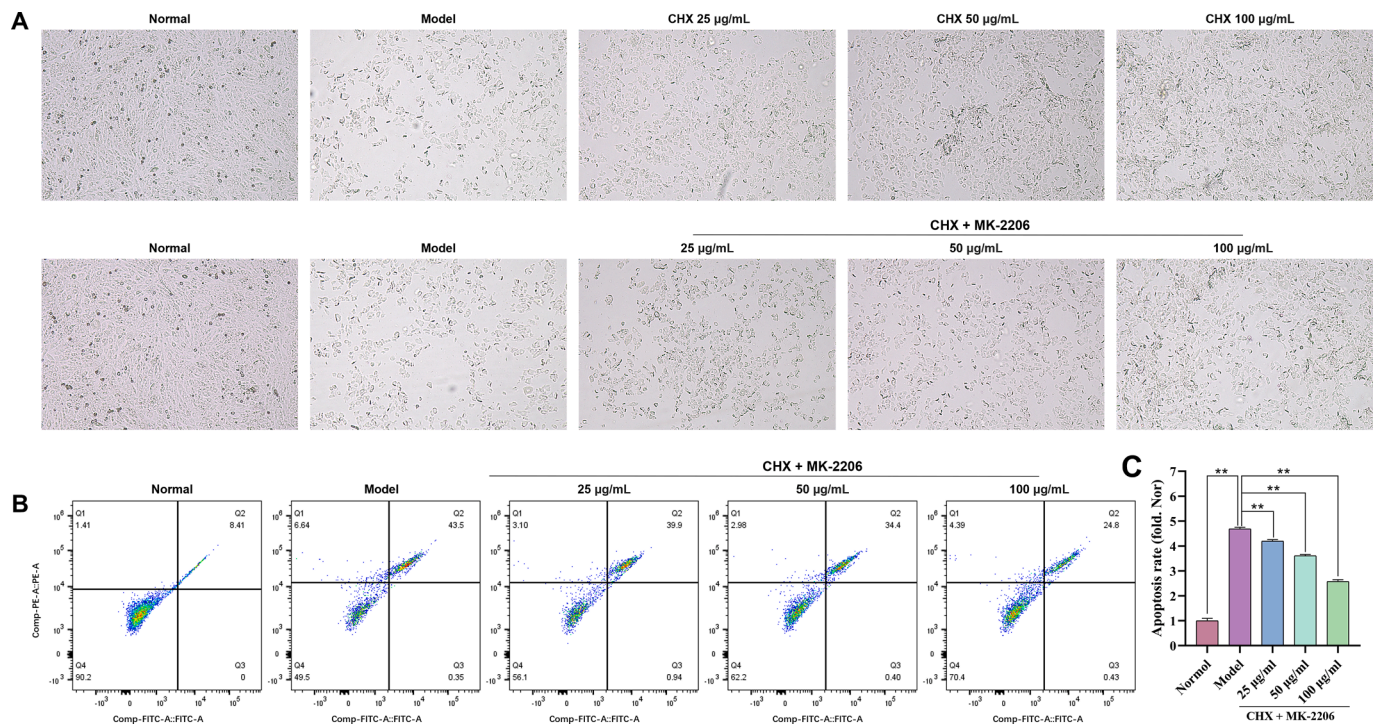


Fig. 10. The effect of Akt inhibitor MK-2206 on the cell protective effect of CHX. (A) MK-2206 reduces the cellular protective effect of CHX. (B)–(C) MK-2206 increases cell apoptosis rate. The data are expressed as the means \pm SDs ($n = 3$). * $p < 0.05$, ** $p < 0.01$, & $p > 0.05$ vs. the Model group.

Program (No. 2022NSFC1593), the National Natural Science Foundation of China (No.82004242), Sichuan Science and Technology Program (No. 2023NSFC180), and the “Xinglin Scholars” discipline talent research promotion project of the Chengdu University of Traditional Chinese Medicine (QJRC2023003).

CRedit authorship contribution statement

Ling-Yu Wang: Data curation, Resources, Visualization, Writing – original draft. **Dan-Dan Tang:** Formal analysis, Software. **Ruo-Lan Li:** Investigation, Supervision. **Mei-Yan Li:** Methodology, Validation. **Li-Sha He:** Conceptualization, Writing – review & editing. **Xu-Feng Pu:** Project administration, Visualization. **Shu-Ting Zhao:** Funding acquisition.

Declaration of competing interest

The authors declare that they have no known competing financial interests or personal relationships that could have appeared to influence the work reported in this paper.

Appendix A. Supplementary data

Supplementary data to this article can be found online at <https://doi.org/10.1016/j.arabjc.2024.105843>.

References

- Bai, W.W., Wang, H., Gao, C.H., Liu, K.Y., Guo, B.X., Jiang, F., Zhang, M.X., Li, C., Qin, W.D., 2021. Continuous Infusion of Angiotensin IV Protects against Acute Myocardial Infarction via the Inhibition of Inflammation and Autophagy. *Oxid Med Cell Longev.* 2021, 2860488. Doi: 10.1155/2021/2860488.
- Bai, M., Pan, C.L., Jiang, G.X., Zhang, Y.M., Zhang, Z., 2019. Effects of Butylphthalide on oxidative stress and inflammatory response in rats with myocardial infarction through Akt/Nrf2 signaling pathway. *Eur Rev Med Pharmacol Sci.* 23 (21), 9642–9650. <https://doi.org/10.26355/eurrev.201911.19458>.
- Beck, S., Martínez Pereyra, V., Seitz, A., Bekeredjian, R., Sechtem, U., Ong, P., 2021. Erkennung ischämietypischer EKG-Veränderungen : Neue Methoden 2021

- [Detection of ECG alterations typical for myocardial ischemia : New methods 2021]. *Internist (berl).* 62 (6), 665–671. <https://doi.org/10.1007/s00108-021-01037-6>.
- Bu, L., Dai, O., Zhou, F., Liu, F., Chen, J.F., Peng, C., Xiong, L., 2020. Traditional Chinese medicine formulas, extracts, and compounds promote angiogenesis. *Biomed Pharmacother.* 132, 110855 <https://doi.org/10.1016/j.biopha.2020.110855>.
- Committee, N.P., 2020. *Chinese Pharmacopoeia Vol. I*, 42–43.
- Fu, W.B., Wang, W.E., Zeng, C.Y., 2019. Wnt signaling pathways in myocardial infarction and the therapeutic effects of Wnt pathway inhibitors. *Acta Pharmacol Sin.* 40 (1), 9–12. <https://doi.org/10.1038/s41401-018-0060-4>.
- Han, X., Qi, J., Yang, Y., Zheng, B., Liu, M., Liu, Y., Li, L., Guan, S., Jia, Q., Chu, L., 2022. Protective mechanisms of 10-gingerol against myocardial ischemia may involve activation of JAK2/STAT3 pathway and regulation of Ca²⁺ homeostasis. *Biomed Pharmacother.* 151, 113082 <https://doi.org/10.1016/j.biopha.2022.113082>.
- Hao, M., Jiao, K., 2022. Jatrotrrhizine reduces myocardial infarction-induced apoptosis and fibrosis through inhibiting p53 and TGF- β /Smad2/3 pathways in mice. *Circ Bras.* 37 (7), e370705.
- Koziolek, M., Alcaro, S., Augustijns, P., Basit, A.W., Grimm, M., Hens, B., Hoad, C.L., Jedamzik, P., Madla, C.M., Maliepaard, M., Mariani, L., Maruca, A., Parrott, N., Pávek, P., Porter, C.J.H., Reppas, C., van Riet-Nales, D., Rubbens, J., Statelova, M., Trevasakis, N.L., Corsetti, M., 2019. The mechanisms of pharmacokinetic food-drug interactions - A perspective from the UNGAP group. *Eur J Pharm Sci.* 134, 31–59. <https://doi.org/10.1016/j.ejps.2019.04.003>.
- Lee, H.G., Jo, J., Hong, H.H., Kim, K.K., Park, J.K., Cho, S.J., Park, C., 2016. State-of-the-art housekeeping proteins for quantitative western blotting: Revisiting the first draft of the human proteome. *Proteomics.* 16 (13), 1863–1867. <https://doi.org/10.1002/pmic.201500344>.
- Li, C.M., Guo, Y.Q., Dong, X.L., Li, H., Wang, B., Wu, J.H., Wong, M.S., Chan, S.W., 2014. Ethanolic extract of rhizome of Ligusticum chuansong Hort. (chuansong) enhances endothelium-dependent vascular reactivity in ovariectomized rats fed with high-fat diet. *Food Funct.* 5 (10), 2475–2485. <https://doi.org/10.1039/c4fo00211c>.
- Li, J., Wang, T., Liu, P., Yang, F., Wang, X., Zheng, W., Sun, W., 2021a. Hesperetin ameliorates hepatic oxidative stress and inflammation via the PI3K/AKT-Nrf2-ARE pathway in oleic acid-induced HepG2 cells and a rat model of high-fat diet-induced NAFLD. *Food Funct.* 12 (9), 3898–3918. <https://doi.org/10.1039/d0fo02736g>.
- Li, J., Liu, H., Yang, Z., Yu, Q., Zhao, L., Wang, Y., 2021b. Synergistic Effects of Cryptotanshinone and Senkyunolide I in Guanxinling Tablet Against Endogenous Thrombus Formation in Zebrafish. *Front Pharmacol.* 11, 622787 <https://doi.org/10.3389/fphar.2020.622787>.
- Li, H., Xia, Z., Chen, Y., Qi, D., Zheng, H., 2018. Mechanism and Therapies of Oxidative Stress-Mediated Cell Death in Ischemia Reperfusion Injury. *Oxid Med Cell Longev.* 2018, 2910643. <https://doi.org/10.1155/2018/2910643>.
- Li, J., Yang, Y., Wang, H., Ma, D., Wang, H., Chu, L., Zhang, Y., Gao, Y., 2022. Baicalein Ameliorates Myocardial Ischemia Through Reduction of Oxidative Stress, Inflammation and Apoptosis via TLR₄/MyD88/MAPK δ /NF- κ B Pathway and Regulation of Ca²⁺ Homeostasis by L-type Ca²⁺ Channels. *Front Pharmacol.* 13, 842723 <https://doi.org/10.3389/fphar.2022.842723>.

- Li, T., Yuan, D., Yuan, J., 2020. Antithrombotic Drugs-Pharmacology and Perspectives. *Adv Exp Med Biol.* 1177, 101–131. https://doi.org/10.1007/978-981-15-2517-9_4.
- Li, S., Zhan, J., Wang, Y., Oduru, P.K., Owusu, F.B., Zhang, J., Leng, L., Li, R., Wei, S., He, J., Wang, Q., 2023. Suxiao Jiuxin Pill attenuates acute myocardial ischemia via regulation of coronary artery tone. *Front Pharmacol.* 14, 1104243. <https://doi.org/10.3389/fphar.2023.1104243>.
- Liao, S., Wu, J., Liu, R., Wang, S., Luo, J., Yang, Y., Qin, Y., Li, T., Zheng, X., Song, J., Zhao, X., Xiao, C., Zhang, Y., Bian, L., Jia, P., Bai, Y., Zheng, X., 2020. A novel compound DBZ ameliorates neuroinflammation in LPS-stimulated microglia and ischemic stroke rats: Role of Akt(Ser473)/GSK3 β (Ser9)-mediated Nrf2 activation. *Redox Biol.* 36, 101644 <https://doi.org/10.1016/j.redox.2020.101644>.
- Liu, D., 2018. Effects of procyanidin on cardiomyocyte apoptosis after myocardial ischemia reperfusion in rats. *BMC Cardiovascular Disorders.* 18 (1), 35. <https://doi.org/10.1186/s12872-018-0772-x>.
- Liu, C.Q., Cao, Y.N., Zuo, Y., Zhang, C.Z., Ren, S.M., Zhang, X., Wang, C.Q., Zeng, Y.J., Leng, J., Liu, Y.L., Chen, Z.X., Cao, X.J., Wu, Z.Z., Zhang, C.T., Lu, J., 2024. Hybridization-based discovery of novel quinoxaline-2-indolinone derivatives as potent and selective PI3Ka inhibitors. *J Adv Res.* <https://doi.org/10.1016/j.jare.2024.03.002>.
- Liu, X., Li, X., Ji, S., Cui, X., Li, M., 2016. Screening of Bioactive Ingredients in Ligusticum Chuanxiong Hort for Protection against Myocardial Ischemia. *Cell Physiol Biochem.* 40 (3–4), 770–780. <https://doi.org/10.1159/000453137>.
- Liu, X., Qi, K., Gong, Y., Long, X., Zhu, S., Lu, F., Lin, K., Xu, J., 2021. Ferulic Acid Alleviates Myocardial Ischemia Reperfusion Injury Via Upregulating AMPK α 2 Expression-Mediated Ferroptosis Depression. *J Cardiovasc Pharmacol.* 79 (4), 489–500. <https://doi.org/10.1097/FJC.0000000000001199>.
- Matta, A., Bouisset, F., Lhermusier, T., Campelo-Parada, F., Elbaz, M., Carrié, D., Roncalli, J., 2020. Coronary Artery Spasm: New Insights. *J Interv Cardiol.* 2020, 5894586. <https://doi.org/10.1155/2020/5894586>.
- Mei, L., Chen, Y., Chen, P., Chen, H., He, S., Jin, C., Wang, Y., Hu, Z., Li, W., Jin, L., Cong, W., Wang, X., Guan, X., 2022. Fibroblast growth factor 7 alleviates myocardial infarction by improving oxidative stress via PI3K/AKT-mediated regulation of Nrf2 and HXK2. *Redox Biol.* 56, 102468 <https://doi.org/10.1016/j.redox.2022.102468>.
- Meyer, I.S., Li, X., Meyer, C., Voloshanenko, A., Pohl, S., Boutros, M., Katus, H.A., Frey, N., Leuschner, F., 2022. Blockade of Wnt Secretion Attenuates Myocardial Ischemia-Reperfusion Injury by Modulating the Inflammatory Response. *Int J Mol Sci.* 23 (20), 12252. <https://doi.org/10.3390/ijms232012252>.
- Ni, Y., Deng, J., Liu, X., Li, Q., Zhang, J., Bai, H., Zhang, J., 2021. Echinacoside reverses myocardial remodeling and improves heart function via regulating SIRT1/FOXO3a/MnSOD axis in HF rats induced by isoproterenol. *J Cell Mol Med.* 25 (1), 203–216. <https://doi.org/10.1111/jcmm.15904>.
- Nusse, R., Clevers, H., 2017. Wnt/ β -Catenin Signaling, Disease, and Emerging Therapeutic Modalities. *Cell.* 169 (6), 985–999. <https://doi.org/10.1016/j.cell.2017.05.016>.
- Pacholewicz, J., Zakliczyński, M., Nożyński, J., Nadziakiewicz, P., Zembala, M., Zembala, M., 2019. Myofibrillarolysis and fibrosis predicts myocardial insufficiency. *Kardiochir Torakochirurgia Pol.* 16 (2), 57–64. <https://doi.org/10.5114/kitp.2019.86356>.
- Pagliari, B.R., Cannata, F., Stefanini, G.G., Bolognese, L., 2020. Myocardial ischemia and coronary disease in heart failure. *Heart Fail Rev.* 25 (1), 53–65. <https://doi.org/10.1007/s10741-019-09831-z>.
- Peng, W., He, C.X., Li, R.L., Qian, D., Wang, L.Y., Chen, W.W., Zhang, Q., Wu, C.J., 2024. Zanthoxylum bungeanum amides ameliorates nonalcoholic fatty liver by regulating gut microbiota and activating AMPK/Nrf2 signaling. *J Ethnopharmacol.* 318, 116848 <https://doi.org/10.1016/j.jep.2023.116848>.
- Qian, W., Xiong, X., Fang, Z., Lu, H., Wang, Z., 2014. Protective effect of tetramethylpyrazine on myocardial ischemia-reperfusion injury. *Evid Based Complement Alternat Med.* 2014, 107501 <https://doi.org/10.1155/2014/107501>.
- Qian, D., Xu, C., He, C.X., Li, M.Y., Guo, J., Zhang, H., 2024. Integration of network pharmacology and bone marrow mesenchymal stem cells experimental research to reveal the molecular mechanisms for Hai Honghua medicinal liquor against osteoporosis. *Integr Med Discov.* 8, e24003. <https://doi.org/10.53388/IMD202408003>.
- Rahman, H., Ryan, M., Lumley, M., Modi, B., McConkey, H., Ellis, H., Scannell, C., Clapp, B., Marber, M., Webb, A., Chiribiri, A., Perera, D., 2019. Coronary Microvascular Dysfunction Is Associated With Myocardial Ischemia and Abnormal Coronary Perfusion During Exercise. *Circulation.* 140 (22), 1805–1816. <https://doi.org/10.1161/CIRCULATIONAHA.119.041595>.
- Salazar, M., Rojo, A.I., Velasco, D., de Sagarra, R.M., Cuadrado, A., 2006. Glycogen synthase kinase-3beta inhibits the xenobiotic and antioxidant cell response by direct phosphorylation and nuclear exclusion of the transcription factor Nrf2. *J Biol Chem.* 281 (21), 14841–14851. <https://doi.org/10.1074/jbc.M513737200>.
- Sarbasov, D.D., Guertin, D.A., Ali, S.M., Sabatini, D.M., 2005. Phosphorylation and regulation of Akt/PKB by the rictor-mTOR complex. *Science.* 307 (5712), 1098–1101. <https://doi.org/10.1126/science.1106148>.
- Şen, S., Karahan, E., Büyükkulaş, C., Polat, Y.O., Üresin, A.Y., 2021. Colchicine for cardiovascular therapy: A drug interaction perspective and a safety meta-analysis. *Anatol J Cardiol.* 25 (11), 753–761. <https://doi.org/10.5152/AnatolJCardiol.2021.707>.
- Shao, C., Wang, J., Tian, J., Tang, Y.D., 2020. Coronary Artery Disease: From Mechanism to Clinical Practice. *Adv Exp Med Biol.* 1177, 1–36. https://doi.org/10.1007/978-981-15-2517-9_1.
- She, Y., Shao, L., Jiao, K., Sun, R., Lang, T., Long, H., Tang, Y., Zhang, W., Ding, C., Deng, C., 2023. Glycosides of Buyang Huanwu decoction inhibits pyroptosis associated with cerebral ischemia-reperfusion through Nrf2-mediated antioxidant signaling pathway both in vivo and in vitro. *Phytomedicine.* 120, 155001 <https://doi.org/10.1016/j.phymed.2023.155001>.
- Shen, Y., Liu, X., Shi, J., Wu, X., 2019. Involvement of Nrf2 in myocardial ischemia and reperfusion injury. *Int J Biol Macromol.* 125, 496–502. <https://doi.org/10.1016/j.ijbiomac.2018.11.190>.
- Stemple, K., DeWitt, K.M., Porter, B.A., Sheeser, M., Blohm, E., Bisanzo, M., 2021. High-dose nitroglycerin infusion for the management of sympathetic crashing acute pulmonary edema (SCAPE): A case series. *Am J Emerg Med.* 44, 262–266. <https://doi.org/10.1016/j.ajem.2020.03.062>.
- Sun, T., Zhang, L., Li, X., Chen, F., Li, Y., Ma, X., Yu, F., 2018. MicroRNA-1 and Circulating Microvesicles Mediate the Protective Effects of Dantonic in Acute Myocardial Infarction Rat Models. *Front Physiol.* 9, 664. <https://doi.org/10.3389/fphys.2018.00664>.
- Tsao, C.W., Aday, A.W., Almarazoo, Z.L., Anderson, C.A.M., Arora, P., Avery, C.L., Baker-Smith, C.M., Beaton, A.Z., Boehme, A.K., Buxton, A.E., Commodore-Mensah, Y., Elkind, M.S.V., Evenson, K.R., Eze-Nliam, C., Fugar, S., Generoso, G., Heard, D.G., Hiremath, S., Ho, J.E., Kalani, R., 2023. American Heart Association Council on Epidemiology and Prevention Statistics Committee and Stroke Statistics Subcommittee. Heart Disease and Stroke Statistics-2023 Update: A Report from the American Heart Association. *Circulation.* 147(8), e93–e621. Doi: 10.1161/CIR.0000000000001123.
- Varasteh, Z., Mohanta, S., Robu, S., Brauer, M., Li, Y., Omidvari, N., Topping, G., Sun, T., Nekolla, S.G., Richter, A., Weber, C., Habench, A., Haberkorn, U.A., Weber, W.A., 2019. Molecular Imaging of Fibroblast Activity After Myocardial Infarction Using a 68Ga-Labeled Fibroblast Activation Protein Inhibitor, FAPI-04. *J Nucl Med.* 60 (12), 1743–1749. <https://doi.org/10.2967/jnumed.119.226993>.
- Wang, C., Peng, D., Liu, Y., Yu, Z., Guo, P., Wei, J., 2020. Agarwood Alcohol Extract Ameliorates Isoproterenol-Induced Myocardial Ischemia by Inhibiting Oxidation and Apoptosis. *Cardiol Res Pract.* 2020, 3640815. <https://doi.org/10.1155/2020/3640815>.
- Wang, W., Shang, W., Zou, J., Liu, K., Liu, M., Qiu, X., Zhang, H., Wang, K., Wang, N., 2022. ZNF667 facilitates angiogenesis after myocardial ischemia through transcriptional regulation of VASH1 and Wnt signaling pathway. *Int J Mol Med.* 50 (4), 129. <https://doi.org/10.3892/ijmm.2022.5185>.
- Wu, Y.Z., Zhang, L., Wu, Z.X., Shan, T.T., Xiong, C., 2019. Berberine Ameliorates Doxorubicin-Induced Cardiotoxicity via a SIRT1/p66Shc-Mediated Pathway. *Oxid Med Cell Longev.* 2019, 2150394. <https://doi.org/10.1155/2019/2150394>.
- Xiao, M., Qian, C., Luo, X., Yang, M., Zhang, Y., Wu, C., Mok, C., Lee, P., Zuo, Z., 2019. Impact of the Chinese herbal medicines on dual antiplatelet therapy with clopidogrel and aspirin: Pharmacokinetics and pharmacodynamics outcomes and related mechanisms in rats. *J Ethnopharmacol.* 235, 100–110. <https://doi.org/10.1016/j.jep.2019.01.040>.
- Xing, Z., Yang, C., He, J., Feng, Y., Li, X., Peng, C., Li, D., 2022. Cardioprotective Effects of Aconite in Isoproterenol-Induced Myocardial Infarction in Rats. *Oxid Med Cell Longev.* 2022, 1090893. <https://doi.org/10.1155/2022/1090893>.
- Yang, Y., Xia, Z., Xu, C., Zhai, C., Yu, X., Li, S., 2022. Ciprofol attenuates the isoproterenol-induced oxidative damage, inflammatory response and cardiomyocyte apoptosis. *Front Pharmacol.* 13, 1037151. <https://doi.org/10.3389/fphar.2022.1037151>.
- Yin, B.Q., Guo, Y.H., Liu, Y., Zhao, Y.Y., Huang, S.M., Wei, X.W., Wang, H.S., Liu, R.Y., Liu, Y., Tang, Y.P., 2021. Molecular mechanism of Chuanxiong Rhizoma in treating coronary artery diseases. *Chin Herb Med.* 13 (3), 396–402. <https://doi.org/10.1016/j.jchmed.2021.03.001>.
- Yu, C., Xiao, J.H., 2021. The Keap1-Nrf2 System: A Mediator between Oxidative Stress and Aging. *Oxid Med Cell Longev.* 2021, 6635460. <https://doi.org/10.1155/2021/6635460>.
- Zhang, Y., Liu, D., Hu, H., Zhang, P., Xie, R., Cui, W., 2019. HIF-1 α /BNIP3 signaling pathway-induced-autophagy plays protective role during myocardial ischemia-reperfusion injury. *Biomed Pharmacother.* 120, 109464 <https://doi.org/10.3390/cells1233726>.
- Zhang, Q., Wang, L., Wang, S., Cheng, H., Xu, L., Pei, G., Wang, Y., Fu, C., Jiang, Y., He, C., Wei, Q., 2022. Signaling pathways and targeted therapy for myocardial infarction. *Signal Transduct Target Ther.* 7 (1), 78. <https://doi.org/10.1038/s41392-022-00925-z>.
- Zhang, Z.G., Zhang, X.L., Wang, X.Y., Luo, Z.R., Song, J.C., 2015. Inhibition of acid sensing ion channel by ligustrazine on angina model in rat. *Am J Transl Res.* 7 (10), 1798–1811. <https://www.ncbi.nlm.nih.gov/pmc/articles/PMC4656758/>.
- Zheng, Q., Huang, Y.Y., Zhu, P.C., Tong, Q., Bao, X.Y., Zhang, Q.H., Zheng, G.Q., Wang, Y., 2018. Ligustrazine Exerts Cardioprotection in Animal Models of Myocardial Ischemia/Reperfusion Injury: Preclinical Evidence and Possible Mechanisms. *Front Pharmacol.* 9, 729. <https://doi.org/10.3389/fphar.2018.00729>.
- Zhou, W.W., Dai, C., Liu, W.Z., Zhang, C., Zhang, Y., Yang, G.S., Guo, Q.H., Li, S., Yang, H.X., Li, A.Y., 2022. Gentianaella acuta improves TAC-induced cardiac remodeling by regulating the Notch and PI3K/Akt/FOXO1/3 pathways. *Biomed Pharmacother.* 154, 113564 <https://doi.org/10.1016/j.biopha.2022.113564>.
- Zhu, L.Y., Wei, Y.H., Wang, Y.H., Li, J.W., Cao, M., Zhou, D., 2022. Protective efficacy of Shenge San on mitochondria in H9c2 cardiomyocytes. *J Tradit Chin Med.* 42 (6), 892–899. <https://doi.org/10.19852/j.cnki.jtcm.2022.06.005>.